1-1-1997

The Nature of Compact Galaxies in the Hubble Deep Field. I. Global Properties

Andrew C. Phillips
University of California, Santa Cruz

Rafael Guzmán
University of California, Santa Cruz

Jesús Gallego
University of California, Santa Cruz

David C. Koo
University of California, Santa Cruz

James D. Lowenthal
University of California, Santa Cruz, jlowenth@smith.edu

See next page for additional authors

THE ASTROPHYSICAL JOURNAL, 489:543–558, 1997 November 10

THE NATURE OF COMPACT GALAXIES IN THE HUBBLE DEEP FIELD. I. GLOBAL PROPERTIES[1,2,3]

ANDREW C. PHILLIPS, RAFAEL GUZMÁN, JESÚS GALLEGO,[4] DAVID C. KOO, JAMES D. LOWENTHAL,[5]
NICOLE P. VOGT, S. M. FABER, AND GARTH D. ILLINGWORTH
UCO/Lick Observatory, Department of Astronomy and Astrophysics, University of California, Santa Cruz, CA 95064;
phillips@ucolick.org, rguzman@ucolick.org, jgm@ucolick.org, koo@ucolick.org, james@ucolick.org, nicole@ucolick.org,
faber@ucolick.org, gdi@ucolick.org
Received 1996 November 6; accepted 1997 June 17

ABSTRACT

We present 10 m Keck spectroscopy and photometry for a sample of 61 small ($r_{1/2} \leq 0\farcs5$), faint ($I_{814} \leq 23.74$), high–surface brightness ($\mu_{I814} < 22.2$ mag arcsec^{-2}) galaxies in fields flanking the Hubble Deep Field. The majority of this empirically defined sample of compact galaxies lies at redshifts $0.4 \lesssim z \lesssim 1$ (88% completeness in redshift identifications), ruling out a large component of low-redshift galaxies. The number of such galaxies in the range $1.4 \lesssim z \lesssim 2.2$ is also constrained to $\lesssim$10%. The majority of the observed galaxies are emission-line systems, while a significant fraction (23%–34%) appear to be normal ellipticals or otherwise early-type systems. One object is an active galactic nucleus, and two are at high redshift ($z > 2$). The Keck redshift and photometric data are combined with *Hubble Space Telescope* images to derive luminosities and physical sizes. We also use emission-line widths, where available, to estimate masses. About two-thirds of the emission-line galaxies, or roughly one-half the sample, are small, low-mass, relatively luminous systems with properties resembling those of local H II galaxies. We compare the properties and numbers of these galaxies to the "bursting dwarf" model of Babul & Ferguson. Our sample includes many galaxies similar to the model galaxies in the redshift range $0.4 \lesssim z \lesssim 0.7$, but the majority of our compact galaxies are more luminous (by up to an order of magnitude) than those of the model. The number of galaxies fitting the model parameters are lower by a factor of 2–3 than predicted. An examination of samples used in analyses of disk surface brightness at redshifts $z > 0.5$ shows that compact galaxies are likely to contribute to the strong disk luminosity evolution found in some studies. Estimates of comoving volume densities indicate that the population of apparent H II galaxies evolves rapidly from redshifts of $z \sim 1$ to the present. It appears that not all of these galaxies can be progenitors of present-day spheroidal galaxies, although the numbers of them with sizes and masses comparable to spheroidals is not dissimilar to estimates of the local field spheroidal density. We also present 51 additional redshifts, acquired for other projects during the same observing period, for a total of 105 objects with identified redshifts $z < 2$ in the Hubble Deep Field and its flanking fields.

Subject headings: cosmology: observations — galaxies: compact — galaxies: distances and redshifts — galaxies: evolution — galaxies: photometry — galaxies: structure

1. INTRODUCTION

The *Hubble Space Telescope* (*HST*) has provided enormous insight into the nature of faint field galaxies through its high angular resolution. In particular, morphological studies have identified a likely major component of the faint blue galaxy excess (see, e.g., Kron 1980; Tyson 1988) as late-type, irregular, and/or peculiar galaxies (Driver, Windhorst, & Griffiths 1995a; Driver et al. 1995b; Glazebrook et al. 1995; Abraham et al. 1996) and have set constraints on the evolution of early-type galaxies (Im et al. 1996; Schade et al. 1996a). However, deep *HST* images also reveal numerous small, high surface brightness, "compact" field galaxies (see Griffiths et al. 1994), for which little morphological information can be gleaned from the images alone. Such faint, compact galaxies are candidates for low-luminosity dwarfs at relatively low redshift (Im et al. 1995), bursting dwarfs at redshifts $z \lesssim 1$ that have faded or disappeared by today (Cowie, Songaila, & Hu 1991; Babul & Rees 1992; Babul & Ferguson 1996), low-luminosity AGNs (Tresse et al. 1996), or smaller premerger components proposed to explain faint galaxy number counts (Guiderdoni & Rocca-Volmerange 1990; Broadhurst, Ellis, & Glazebrook 1992) or as part of hierarchical clustering models (Kauffmann et al. 1993; Cole et al. 1994). Faint compact galaxies are also likely to include more examples of the moderate-redshift compact narrow-emission-line galaxies (CNELGs; Koo et al. 1994, 1995; Guzmán et al. 1996). Because of their small angular sizes, the nature of these faint compact galaxies is best revealed through spectroscopy, which provides redshifts (and hence luminosities and physical sizes), stellar population information, internal kinematics, conditions of the ISM, and star formation rates.

In this pair of papers, we present spectroscopy and photometry of a sample of compact galaxies in the flanking fields of the Hubble Deep Field (HDF; Williams et al. 1996). We define "compact" on purely empirical grounds—the objects have small angular size (half-light radius $r_{1/2} \leq 0\farcs5$) and relatively high surface brightness ($\leq$22.2 mag arcsec^{-1} I-band). The present paper discusses the global properties

[1] Based on observations obtained at the W. M. Keck Observatory, which is operated jointly by the California Institute of Technology and the University of California.

[2] Based in part on observations with the NASA/ESA *Hubble Space Telescope*, obtained at the Space Telescope Science Institute, which is operated by AURA, Inc., under NASA contract NAS 5-26555.

[3] Lick Observatory Bulletin 1361.

[4] Departamento de Astrofisica, Universidad Complutense de Madrid, E-28040 Spain.

[5] Hubble Fellow.

of these galaxies: redshift distribution, luminosities, sizes, and masses. The sample selection, observations, and many of the analysis techniques are discussed in § 2. The properties of the sample are described in § 3. Section 4 discusses how these galaxies compare to other observations and the predictions of models. Notes on individual objects, as well as a summary table of redshifts for 51 additional HDF galaxies not part of the compact sample, are included in the Appendix.

Guzmán et al. (1997a, hereafter Paper II) discuss spectral line diagnostics, star formation rates, and the significance of these galaxies to the evolution of the general galaxy population.

This work is part of the DEEP project (Koo 1995). We adopt $H_0 = 50$ km s^{-1} Mpc^{-1} and $q_0 = 0.05$ throughout, unless otherwise stated. All magnitudes are on the Vega-based system.

2. OBSERVATIONS, DATA, AND REDUCTION PROCEDURES

2.1. *Sample Selection and Size Measurements*

The original targets were selected on the basis of high surface brightness within the half-light radius. For the initial selection of targets, photometry of all the HDF flanking fields was performed with automated algorithms, measuring the light in a series of circular apertures $\leq 3''$ diameter, to derive total magnitudes and half-light radii. The effects of neighboring objects were identified by slope changes in the curve of growth, and corrections were applied. Objects brighter than $I_{814} = 23.74$ (978 in total) and with surface brightness above 22.24 mag arcsec^{-2} (388 objects) were retained as possible compact targets.

These targets represent galaxies in the upper $\sim 37\%$ in surface brightness. Fifty-three objects which followed an obvious stellar sequence ($r_{1/2} < 0''.16$) were removed from the target pool. Objects that appeared on target lists for other programs (54, consisting mostly of galaxy candidates and highly inclined disks) were also removed from the pool; we will consider the effects of this exclusion below. Targets were selected for spectroscopy from this remaining pool (Fig. 1*a*), with a slight preference given to objects with the highest surface brightness. There was no preference based on magnitude.

Following the observations, the *HST* I_{814}-band images of observed objects were reanalyzed in more detail than was feasible to do for the entire catalog (see § 2.3 below). We found a few instances where, on the basis of the automated photometry, we had selected features such as bars within large spirals which completely filled the $3''$ aperture, and highly inclined disk galaxies of fairly large major-axis extent. These galaxies are easy to identify morphologically as elliptical or disk galaxies and are not "compact" in the sense of small angular size. In fact, we found that objects with major-axis radii $a_{1/2} > 0''.5$ could be readily identified morphologically in the *HST* images. We therefore added an upper angular size limit of $a_{1/2} = 0''.5$ to define the final sample of 63 observed compact objects shown in Figure 1*b*. The surface brightness has been calculated using the semimajor axis radius, following Kent (1985). The corresponding number of potential targets following the final size cut is estimated to be ~ 245. The corresponding number of galaxies in the $I_{814} \leq 23.74$ catalog meeting the final size criteria, but of any surface brightness, is ~ 560.

Within our other scientific projects from this run, we observed nine objects—mostly elliptical galaxy candidates—that fit our compact galaxy criteria. These observations will be presented in detail elsewhere, but the galaxies are included in this paper for purposes of statistical analysis (see § 3.1). We also searched the HDF redshift data published by Cohen et al. (1996) for other compact galaxies, finding eight additional galaxies that pass our final criteria. We have included these galaxies in our discussion whenever possible. However, as we do not know the selection criteria

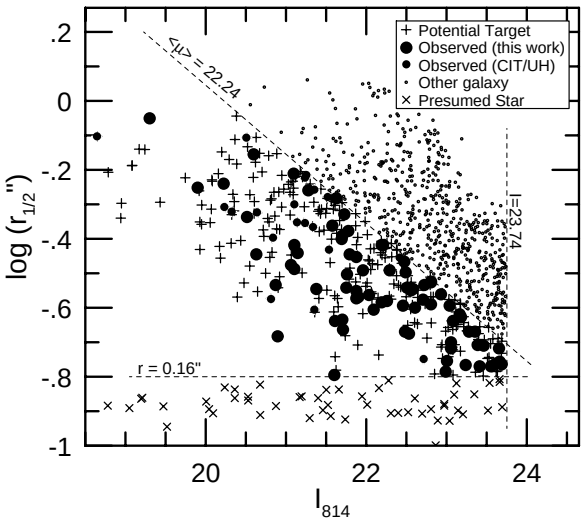

FIG. 1*a*

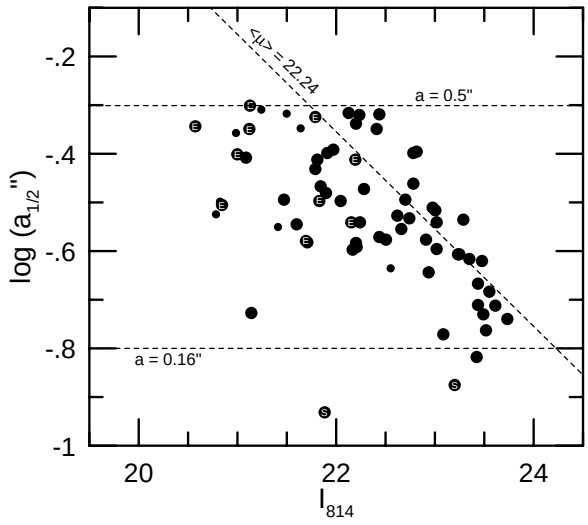

FIG. 1*b*

FIG. 1.—(*a*) Original sample selection. The pool of potential compact objects was chosen to have surface brightnesses within the I_{814} half-light radius, $r_{1/2}$, of $\langle\mu\rangle \leq 22.24$ mag arcsec^{-2}. Objects were measured with an automated procedure in $\leq 3''$ diameter circular apertures. Objects believed to be stars ($r_{1/2} < 0''.16$) were excluded. There was also a cutoff in magnitude at $I_{814} = 23.74$. The objects actually observed by us and others (Cohen et al. 1996) are indicated. (*b*) Half-light semimajor axis plotted against final I_{814} magnitude for the observed sample of compact targets. These are independent measurements made following the observations, using isophotal elliptical apertures and masking out neighboring objects. We use the half-light semimajor axis, $a_{1/2}$, as a more stringent criterion for compactness, since highly inclined disks may have a small circular half-light radius and yet are easily identified morphologically. Note that the two smallest objects have been identified spectroscopically as stars (S). The objects identified as early-type galaxies are marked with (E).

or redshift detection rate for these galaxies, they must be excluded from any statistical analysis.

2.2. *Spectroscopic and Photometric Observations*

Spectroscopic observations were made over the nights of 1996 April 22–24 UT, using the 10 m W. M. Keck telescope and the Low-Resolution Imaging Spectrograph (LRIS; Oke et al. 1995). LRIS is a multiobject spectrograph which uses slitmasks to provide nearly 8′ of available slit length on the sky; for these observations, we covered 30–40 objects with a single slit mask. Primary science goals targeted objects in the HDF itself, leaving much of the slit mask space in the flanking fields available for observations of compact objects. For each slit mask, we obtained a pair of 1500 s exposures with each of the 600 line millimeter^{-1} red and 600 line millimeter^{-1} blue gratings, providing continuous spectral coverage from about 4000–8500 Å at 1.26 Å pixel^{-1}. The effective resolution, which depends on the slit width (1″.1), object size, and Keck seeing ($\sim$0″.9), was about 3.1 Å FWHM for stars (see § 3.5 below). Most compact galaxies were observed through only one slit mask, for a total exposure time of 3000 s. The length of each slitlet was greater than 8″ in almost all cases, providing adequate room for sky subtraction after accounting for seeing and object size.

The flanking fields were imaged by *HST* through only the F814W filter ("I_{814}"). We also obtained two 300 s V-band exposures with LRIS in direct imaging mode, in order to provide some color information for the compact galaxies. These images were calibrated using published V_{606}- and I_{814}-band photometry in the HDF itself (Williams et al. 1996). To derive colors, we degraded the *HST* I_{814} images to match the ground-based seeing and performed photometry in identical 1″.12 radius apertures on both the LRIS V and degraded *HST* I_{814} images. From the $V_{\rm LRIS}$ to V_{606} relation measured from galaxies in the HDF and from comparison between our two LRIS images, we estimate the typical error in $(V_{606} - I_{814})$ to be 0.15 mag.

2.3. *HST Image Analysis*

Using the STSDAS ISOPHOTE package, we fitted a series of isophotal ellipses to each image out to 8″ and constructed a curve of growth for fluxes within those elliptical apertures. This was used to derive an asymptotic "total" I_{814} magnitude and a major-axis half-light radius. During this process, images of neighboring galaxies were masked out. We also attempted to characterize the major-axis profile as exponential or $r^{1/4}$-law, but in many cases the spatial resolution was too poor to do this convincingly.

Comparison of the original photometry used for sample selection and the final photometry showed good agreement (0.02 ± 0.12 mag rms) in the derived total magnitudes. A slight offset was seen in the half-light radii, with the semimajor axis radii larger than the preliminary circular $r_{1/2}$ by a median amount of 17%, consistent with a median ellipticity of $\sim$0.28. A few larger noncompact objects showed significant deviations, mostly because they were too large for the 3″ diameter aperture used in the original photometry.

2.4. *Effects of WFPC2 PSF on Half-Light Radii*

Since the objects in this study are so small in angular size, the WFPC2 Point Spread Function (PSF) may have a systematic effect on the measurement of half-light radii. In order to test this, we constructed several model galaxies of standard forms (de Vaucouleurs ellipticals and exponential disks) using the IRAF ARTDATA package. The models, of galaxy sizes relevant to this study, were constructed at a pixel scale of 0″.025 pixel^{-1} and rebinned to the Wide Field Camera scale, 0″.1 pixel^{-1}. We measured these using the same methods as for our sample galaxies and compared the input models and measured half-light radii, as shown in Figure 2*a*. The good agreement between the model input and the measured radii verifies the image analysis technique used above. We then convolved the model galaxy images with a model PSF constructed using TinyTim v4.0 (see Krist 1993); the convolution was performed before rebinning to avoid undersampling the PSF. These images were then scaled to intensities typical for the flanking field images and appropriate noise was added. The final images were analyzed and the half-light radii compared (Fig. 2*b*). At radii larger than $\sim$0″.4, effects of the PSF on size measurements are small (<10%), but at smaller radii the measurements become systematically too large. In particular, the three point sources have measured half-light radii of 0″.14 $\pm$ 0″.02. We find that, to first order, the measured half-light radii can be restored to the input values by subtracting 0″.15 in quadrature. The measured radii thus "corrected" are shown in Figure 2*c*. This correction has been adopted in our subsequent analysis.

These tests also provide a check on the accuracy of our method of photometry. The model galaxies all have the

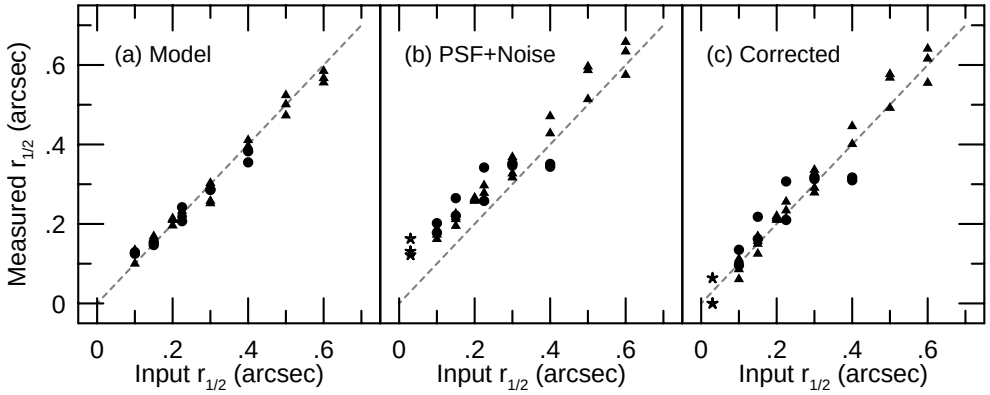

FIG. 2.—Measured half-light radii compared to input radii in model galaxy images, before and after degradation with a WFPC2 PSF and noise (*a* and *b*, respectively). Symbols denote $r^{1/4}$-law profiles (*filled circles*), exponential disks (*filled triangles*) and point sources (*five-pointed stars*). In (*b*), the systematic trend toward measurements which are too large at small radii is attributed to the effects of the PSF. This trend can be corrected to first order by subtracting a small constant, 0″.15, in quadrature, as shown in (*c*).

same input counts, corresponding to a magnitude of 21.703. The total measured magnitudes were 21.701 ± 0.027 (standard deviation) in the nondegraded models; the same models degraded with the PSF and noise were measured at 21.735 ± 0.068 mag.

3. RESULTS

The final observed sample consists of the 63 objects shown in Figure 3 (Plate 8). The median measured properties are $a_{1/2} = 0\farcs30$ and $I_{814} = 22.41$. Reasonably secure spectral identifications could be made for 56 objects, for an overall redshift completeness of 88%. The identifications include two late-type stars, two high-redshift objects at $z = 2.269$ and 2.990, and one AGN with broad Mg II emission at $z = 0.960$. Redshifts for the remaining 51 objects were derived primarily from [O II] λ3727 for emission-line systems and Ca II H + K for absorption-line systems. All identifications were based on at least two lines, although this was sometimes limited to the marginally resolved [O II] doublet.

The seven objects for which no redshifts could be identified all have reasonably strong continua. Four of the seven have ground-based V photometry (the others fell outside the direct image fields). Two of these show relatively red ($V_{606} - I_{814}$) colors consistent only with early-type galaxies at $z \sim 1$, and the other two show colors consistent with an intermediate stellar population at a similar redshift (although the colors are not unique in this latter case). An alternative, that the unidentified objects are halo dwarf stars, is ruled out for all but one object by their extended images. The one possible stellar object, in fact, has a spectral shape rather similar to high-redshift objects, showing what appears to be a Lyα break at $z \sim 3.5$, but we have been unable to make a convincing match to specific spectral features, nor is its color ($V_{606} - I_{814} = 1.16$) particularly suggestive of such high redshift (see Lowenthal et al. 1997).

The total compact object sample is listed in Table 1, along with basic measurements (coordinates, redshift, I_{814} magnitude, V_{606}–I_{814} color and half-light radius), derived rest frame parameters (B-band luminosity, size), and velocity width. For the eight compact galaxies observed by others, we have photometry, size measurements, and redshifts but no other spectral information. Notes on selected objects with unusual spectra are provided in the Appendix.

3.1. *General Spectral Properties*

Fifty-one of the 54 compact galaxies with redshift identifications lie at redshifts $z < 2$ and display no spectral evidence for AGNs. These galaxies, which make up $\sim$95% of

TABLE 1

MEASURED PARAMETERS OF THE SAMPLE GALAXIES

Object (1)	α_{2000} (2)	δ_{2000} (3)	z (4)	I_{814} (5)	$V-I$ (6)	$a_{1/2}$ (7)	R_e (8)	M_B (9)	σ (10)	Notes (11)
ow3_0959_0445.....	12 36 24.59	62 14 19.7	...	23.61	...	0.19	...	...	...	
ow3_1308_0563.....	12 36 25.05	62 13 43.2	0.654	23.73	0.93	0.18	0.93	−18.66	63	
ow3_1047_0444.....	12 36 25.10	62 14 11.7	0.318	22.91	...	0.26	1.34	...	37	
ow2_0156_0020.....	12 36 25.52	62 15 50.0	...	21.71	...	0.26	...	...	...	
ow3_1377_0542.....	12 36 25.72	62 13 37.8	...	23.42	1.16	0.15	...	...	...	
ow3_1063_0391.....	12 36 25.89	62 14 12.4	0.528	23.23	0.57	0.25	1.61	−18.66	50	
iw4_1002_1353	12 36 27.24	62 12 58.9	1.221	22.17	0.91	0.25	2.27	−22.50	77	
iw4_1173_1391	12 36 27.73	62 12 41.8	0.519	20.84	1.51	0.31	2.22	−20.56	...	E
sw4_0807_1067	12 36 28.36	62 10 38.1	0.760	22.24	0.92	0.29	2.36	−20.55	61	
iw4_1212_1333	12 36 28.70	62 12 40.6	0.880	23.55	0.62	0.21	1.45	−19.69	53	
ow3_1376_0297.....	12 36 28.91	62 13 47.7	0.693	22.28	1.03	0.34	2.80	−20.25	44	
sw4_1068_1043	12 36 30.17	62 10 15.3	0.482	21.90	0.77	0.33	2.30	−19.72	45	
iw2_0497_0674	12 36 33.19	62 14 12.2	1.344	23.00	0.55	0.30	3.01	−21.74	75	
iw2_0186_0458	12 36 34.22	62 14 49.2	0.507	22.41	0.82	0.45	3.37	−19.32	$\leq$35	
sw3_1055_0618	12 36 35.63	62 10 33.6	...	23.48	...	0.24	...	...	...	
iw3_0817_0556	12 36 36.57	62 13 47.8	0.960	21.14	0.71	0.19	1.16	−22.42	127	A
iw4_1499_0841	12 36 36.77	62 12 34.2	0.437	23.02	0.83	0.29	1.82	−18.27	37	
se4_0940_1478.....	12 36 37.95	62 09 29.0	0.513	22.62	...	0.30	2.07	...	47	
iw2_0547_0293	12 36 38.45	62 14 22.9	2.990	23.52	0.65	0.17	1.22	−23.50	...	
iw2_0242_0156	12 36 38.48	62 14 56.3	...	22.70	1.31	0.32	...	...	...	
iw2_0106_0094	12 36 38.52	62 15 11.1	0.462	23.09	0.85	0.17	0.76	−18.35	45	
sw3_1378_0453	12 36 39.63	62 10 10.8	0.509	21.12	1.18	0.45	3.39	−20.39	$\leq$35	E
sw3_1455_0476	12 36 39.78	62 10 02.8	0.137	21.79	0.31	0.37	1.11	−17.00	$\leq$35	
iw3_1144_0405	12 36 40.41	62 13 24.1	0.485	23.35	0.87	0.24	1.49	−18.22	41	
nw4_0989_1527.....	12 36 40.89	62 15 01.8	0.000	21.88	1.73	0.12	...	...	...	
se2_0021_0728.....	12 36 42.44	62 11 22.8	0.845[a]	22.20	0.92	0.46	4.33	−20.90	65	
nw4_0770_1239.....	12 36 43.39	62 15 33.3	0.847	22.13	1.05	0.48	4.60	−20.99	72	
nw4_0920_1247.....	12 36 44.16	62 15 19.4	0.570	22.21	0.99	0.26	1.76	−19.77	$\leq$35	
se2_0309_0594.....	12 36 45.84	62 11 01.9	0.936	21.79	2.00	0.47	4.64	−21.96	128	E
nw4_0882_1069.....	12 36 46.26	62 15 30.0	...	22.20	2.06	0.26	...	...	...	
nw4_1278_1205.....	12 36 46.76	62 14 48.4	0.558	20.57	1.58	0.45	3.59	−21.06	...	E
se4_1387_0990.....	12 36 46.86	62 09 07.8	0.905	22.78	1.04	0.40	3.78	−20.59	109	
nw2_0367_0766.....	12 36 47.26	62 16 29.1	0.873	21.00	2.05	0.40	3.72	−22.41	...	E
nw4_1111_0965.....	12 36 48.93	62 15 13.3	0.457	22.44	0.80	0.27	1.68	−19.00	63	
nw2_0557_0629.....	12 36 50.14	62 16 17.3	0.503	22.15	1.30	0.29	1.96	−19.25	...	E
se2_0673_0133.....	12 36 53.93	62 10 47.3	0.594	22.44	0.71	0.48	3.95	−19.73	68	
se3_0982_0226.....	12 36 54.49	62 10 15.5	0.224	23.44	0.66	0.22	0.74	−16.20	41	
se3_1090_0023.....	12 36 57.76	62 10 13.8	0.410	21.83	0.82	0.32	2.01	−19.28	...	E
ie4_1144_1033	12 37 00.67	62 11 37.7	0.000	23.20	1.56	0.13	...	...	...	
nw3_1434_0108.....	12 37 01.98	62 15 18.3	0.744	22.82	1.15	0.40	3.57	−19.90	112	

TABLE 1—*Continued*

Object (1)	α_{2000} (2)	δ_{2000} (3)	z (4)	I_{814} (5)	$V-I$ (6)	$a_{1/2}$ (7)	R_e (8)	M_B (9)	σ (10)	Notes (11)
ie4_1442_1007	12 37 02.72	62 11 11.5	0.560	21.13	1.26	0.50	4.02	−20.66	117	E
ne4_1136_1005	12 37 02.80	62 14 28.8	0.898	22.94	1.12	0.23	1.74	−20.41	65	
ne4_1292_0943	12 37 04.50	62 14 17.1	1.050	23.29	0.69	0.29	2.68	−20.60	43	
ne3_0769_0583	12 37 06.20	62 15 19.1	0.840	21.60	0.78	0.28	2.42	−21.49	109	
ie3_1030_0507	12 37 06.86	62 12 09.2	0.693	23.44	1.00	0.19	1.15	−19.10	47	
ie_0998_0401	12 37 08.07	62 12 16.4	0.594	21.81	1.01	0.39	3.10	−20.28	91	
ne3_0969_0527	12 37 08.08	62 15 03.1	0.570	22.19	1.60	0.39	3.04	−19.51	79	E
ie3_1443_0559	12 37 08.56	62 11 29.5	0.907	21.91	0.76	0.40	3.79	−21.44	61	
ie2_0623_0190	12 37 08.66	62 12 59.0	2.269	23.25	0.49	0.25	2.39	−23.04	...	
ie3_1025_0359	12 37 08.77	62 12 15.6	0.788	23.49	0.83	0.19	1.07	−19.40	53	
ie3_1071_0351	12 37 09.13	62 12 11.7	0.476	22.98	0.85	0.31	2.09	−18.54	≤ 35	
ne3_1126_0494	12 37 09.41	62 14 50.2	0.420	22.66	0.84	0.28	1.70	−18.50	51	
ne3_1323_0484	12 37 10.67	62 14 32.6	0.677	21.69	1.83	0.26	1.99	−20.60	...	E
oe4_1100_1320	12 37 10.92	62 10 49.4	0.483	23.02	...	0.25	1.60	...	43	
oe4_1109_1148	12 37 13.21	62 10 55.5	0.936	21.47	0.86	0.32	2.94	−22.00	151	
oe4_1223_1134	12 37 14.04	62 10 45.6	0.821	22.05	0.83	0.32	2.79	−20.96	68	
oe2_0342_0725	12 37 14.32	62 12 22.3	1.084	22.74	1.22	0.29	2.73	−21.56	84	
oe2_0458_0695	12 37 15.38	62 12 13.0	...	22.50	1.91	0.26	...	...	...	
oe2_0040_0229	12 37 19.05	62 13 09.8	0.423	22.78	0.93	0.35	2.27	−18.32	78	
oe2_0168_0249	12 37 19.53	62 12 57.3	0.909	22.23	1.39	0.48	4.65	−21.25	69	
oe2_0513_0235	12 37 21.69	62 12 26.4	0.480	21.09	1.06	0.39	2.81	−20.31	97	
oe3_1089_0455	12 37 22.13	62 11 25.1	0.784	21.84	1.14	0.34	2.99	−21.04	64	
oe3_0801_0291	12 37 22.61	62 11 57.9	0.487	21.97	0.99	0.41	2.96	−19.52	69	
Compact Galaxies from Other Sources										
iw4_1173_1391	12 36 27.73	62 12 41.8	0.518	20.82	1.55	0.32	2.27	−20.55	...	
iw4_1214_1375	12 36 28.17	62 12 38.8	0.518	20.98	1.08	0.44	3.34	−20.65	...	
ow3_1251_0168.....	12 36 29.87	62 14 04.3	0.793	21.64	1.21	0.45	4.13	−21.28	...	
iw4_1290_1130	12 36 31.80	62 12 41.7	0.528	21.24	0.89	0.49	3.82	−20.57	...	
nw3_1040_0220.....	12 36 58.26	62 15 49.7	0.457	20.78	0.68	0.30	1.96	−20.75	...	
ne2_0657_0709	12 37 03.91	62 15 24.3	0.377	21.50	0.88	0.48	3.11	−19.30	...	
ne2_0469_0546	12 37 04.95	62 15 48.0	0.533	22.55	0.81	0.23	1.44	−19.32	...	
ie3_0984_0464	12 37 07.17	62 12 15.1	0.655	21.41	1.87	0.28	2.15	−20.74	...	

NOTES—Col. (1): Object ID: (field, CCD)_(x)_(y), with x and y in pixels. Cols. (2) and (3): J2000.0 coordinates. Units of right ascension are hours, minutes, and seconds, and units of declination are degrees, arcminues, and arcseconds. Col. (4): Redshift. Col. (5): Total I_{814} magnitude. Col. (6): Total ($V-I_{814}$) color. Col. (7): Measured half-light semimajor axis (arcsec)—no PSF correction applied. Col. (8): Half-light radius (kpc) from col. (7), corrected for PSF and for $H_0 = 50$ km s^{-1} Mpc^{-1} and $q_0 = 0.05$. Col. (9): Luminosity. Col. (10): Line width (Gaussian sigma), in km s^{-1}. Col. (11): E = early-type galaxy; A = AGN.

[a] Also shows emission system at $z = 0.912$.

our identified galaxy sample, are the focus of our investigation into the nature of compact galaxies. Examination of the spectra reveals four objects with no detectable emission lines but generally strong Ca II H + K breaks typical of elliptical galaxies. Five more have relatively weak emission lines ($W_\lambda 3727 < 20$ Å) and again have relatively strong H + K breaks. These spectra are typical of local spiral galaxies of Hubble types SBc and earlier (Kennicutt 1992), including many elliptical galaxies. We will refer to these continuum-dominated spectra as "early type."

It is not surprising to find a number of elliptical or bulge-dominated galaxies among the compact galaxies; these galaxies are strongly concentrated in their central regions so that the average surface brightness within the half-light radius is quite high (see, e.g., Kent 1985). Furthermore, surface brightness increases with decreasing effective radius among luminous ellipticals (Kormendy 1985), so that the ellipticals most likely to satisfy the surface-brightness cutoff will also be the smallest. In fact, about 25 galaxies were removed from the target pool of compact galaxies based on their elliptical appearance (§ 2.1); had these been included, we might have expected $25 \times (63/245) \simeq 6$ to fall in our sample. Among the nine galaxies actually observed from this excluded sample for other science programs, seven proved to be early-type, one was a small inclined disk, and one was a strong emission-line object at $z = 0.136$.

As noted above, some or all of the seven unidentified galaxies in our compact sample may be early-type absorption or weak emission line systems. Therefore, between nine and 16, or 15%–26%, of the observed sample of 61 galaxies appear to be normal early-type systems. Since the majority of the excluded galaxies were thought to be ellipticals, we need to make a correction to this percentage. To first order, we may do this by adding the nine galaxies from that sample which were actually observed (comparable to the six we might have expected to observe if these galaxies had not been excluded). Adding these galaxies, the number of early-type galaxies becomes 16 to 23 out of 70, or 23%–33%.

Most of the remaining galaxies have strong emission lines ($W_\lambda 3727 \gg 20$ Å), consistent with later type, star-forming galaxies (Kennicutt 1992). The spectral properties and star formation rates of these objects are discussed in Paper II.

3.2. *Redshifts*

The redshift distribution of the sample, compared with all HDF redshifts to date, is shown in Figure 4. Sources for the total sample are Cohen et al. (1996); Moustakas, Zepf, & Davis (1997); Steidel et al. (1996); and redshifts from the DEEP project published here and in Lowenthal et al. (1997). We caution that the total redshift sample is not necessarily representative of the general galaxy distribution,

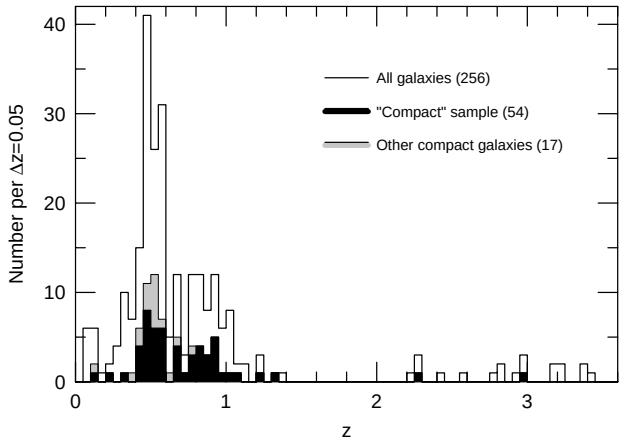

FIG. 4.—Distribution of redshifts of the compact galaxies compared to other galaxies in the HDF, compiled from several sources (see text). The scarcity of compact objects at low redshift is probably caused by our cutoff in angular half-light radius, $a_{1/2} \leq 0\farcs5$, whereas at $z > 2$ we expect few galaxies to meet our surface-brightness criteria because cosmological dimming becomes severe. Otherwise, the compact galaxies show a generally similar redshift distribution to the other galaxies, although with somewhat less concentration in redshift "spikes."

since target selection varied from group to group and often focused on preselected groups of galaxies, such as the color-selected $z > 2$ candidates (Steidel et al. 1996; Lowenthal et al. 1997). Furthermore, some galaxies in the HDF itself may fit our criteria for compact galaxies (however, none of the 12 objects in Fig. 4 from the Lowenthal et al. sample fit our specific criteria).

The sample of compact galaxies appears deficient in both low-redshift ($z < 0.4$) and high-redshift ($z > 2$) galaxies compared to the total HDF sample. Some of this is because of bias in the total sample (e.g., an emphasis on preselected $z > 2$ targets), and some is because of our selection criteria. For example, at $z = 0.2$, our maximum size of $a_{1/2} = 0\farcs5$ eliminates all galaxies larger than $R_e = 1$ kpc from our compact sample. On the other hand, cosmological dimming quickly becomes severe at redshifts above $z \sim 1$, which means our surface brightness cutoff will tend to exclude high-z objects.

Within the range $0.4 \lesssim z \lesssim 1.2$, we find the redshift distribution of the compact objects follows the peaks and valleys of the total sample fairly well. There is a suggestion that the compact galaxies are less likely than other galaxies to fall in redshift "spikes," such as those at, e.g., $z = 0.475$ and 0.559 (Cohen et al. 1996). Cohen et al. find 54 out of 140 HDF galaxies, or ~39%, in six such peaks; statistically, we might expect 18 of our galaxies to lie in the same structures. In fact, we observe only eight, a difference significant at a greater than 99% confidence level.

To further quantify these points, we ran a double-sided K-S test on the distributions of the compact galaxies versus the remaining sample (excluding the $z > 2$ objects), which we refer to as the "noncompact" sample. The probability that the two samples are not drawn from the same population is 88%. However, restricting both samples to $z \geq 0.4$ (where our compact sample will not suffer strong biases) and reducing by one-half the number of galaxies in each redshift spike of Cohen et al. (1996) brings this likelihood to only 3%—that is, there is a 97% probability that the compact sample could have come from the same parent population as the noncompact galaxies, were it not for clumping in redshift spikes in the noncompact galaxies. This demonstrates both the general similarity of the redshift distributions for redshifts $z \geq 0.4$ and the difference of concentration in redshift structures between the compact and noncompact galaxy samples.

We do see a fairly sharp drop in the number of compact galaxies above $z \sim 1$, which may seem important in testing the "bursting dwarf" hypothesis (see § 4 below), but the drop appears reflected in the noncompact sample as well and is almost certainly caused by selection biases in our redshift identifications. For example, we are largely insensitive to redshifts $z \gtrsim 1.4$, where the [O II] λ3727 line falls beyond the observed spectral range, and thus any identifications must be made using relatively weak UV absorption features of Mg II and Fe II (in fact, we have no secure redshifts in this range). For redshifts beyond $z = 0.95$, λ3727 enters the wavelength region of intense night-sky emission, so that weak [O II] may easily be missed. It is similarly difficult to make identifications of absorption-line spectra at $z \gtrsim 0.85$, when the 4000 Å break enters the night sky forest. For star-forming galaxies, we recover some sensitivity beyond $z \gtrsim 2.2$, when Lyα enters our range of spectra. However, there cannot be a large population of sample galaxies in the range $1.4 \lesssim z \lesssim 2.2$, since only seven objects out of 63 (11%) remain unidentified.

3.3. *Colors and Luminosities*

The compact galaxies span a range in color, $0.32 \leq V_{606} - I_{814} \leq 2.05$. Figure 5 shows the colors plotted against redshift. The reddest galaxies have $z \sim 0.8$, whereas the bluest span the entire range of observed redshift. Most of the galaxies form a broad band at nearly constant $V_{606} - I_{814} \sim 0.9$, while those with early-type spectra form a reasonably tight red sequence.

In order to show the expected color behavior for galaxies of different types, we have taken three representative spectral energy distributions (SEDs) and calculated $V_{606} - I_{814}$ as the spectra are shifted through our photometric pass-

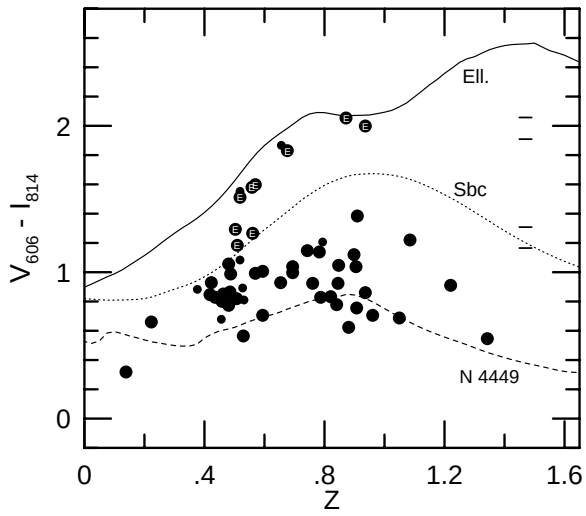

FIG. 5.—$V_{606} - I_{814}$ color as a function of redshift. The tracks of local elliptical, SBc, and starburst (NGC 4449) galaxies are based on observed SEDs (no color evolution). Most of our galaxies lie in the region occupied by local star-forming galaxies, with a significant fraction having similar colors to NGC 4449. The continuum-dominated systems (E), not unexpectedly, fall near the track of the local elliptical SED. Symbols are as in Fig. 1; horizontal bars mark the colors of the four sample galaxies with measured $V_{606} - I_{814}$ but no redshift identifications.

bands. The SEDs are those of a local elliptical galaxy (Bruzual & Charlot 1993); an intermediate spiral (SBc, from Coleman, Wu, & Weedman 1980); and the starburst galaxy NGC 4449 (R. E. Ellis & A. G. Bruzual 1983, private communication). The resulting tracks are overlaid in the figure. The bulk of the compacts lie on or just redward of the starburst curve, agreeing with the spectroscopic identification of actively star-forming galaxies based on the presence of strong emission lines (also see Paper II). Thus, the majority of the compact galaxies belong to the "faint blue galaxy" population. The spectroscopically identified early-type galaxies lie between the SBc and elliptical tracks, with an upper envelope just blueward of the elliptical track, as expected for a passively evolving stellar population.

Redshifts allow us to estimate luminosities from apparent magnitude, adopting k corrections based on measured $V_{606} - I_{814}$ colors. For this purpose, we used the 11 model SEDs of Gronwall & Koo (1995; see also Gronwall 1996), which provide a finer sampling of the color-redshift space than the three SEDs above. No evolution with redshift is included in these SEDs. Since most of the compact galaxies lie in the redshift range where the B-band corresponds to the observed V through I_{814} range ($0.25 \lesssim z \lesssim 0.85$), the k corrections should be well constrained. The distribution of luminosities as a function of redshift is shown in Figure 6. The selection cutoff of $I_{814} < 23.74$ is shown for the reddest and bluest SEDs. The galaxies span a range of nearly 7 mag in M_B, with luminosity and redshift strongly correlated because of the magnitude selection criterion. We might expect that the compact galaxies at $z \sim 1$, which tend to be L^* galaxies, would have little in common with those at $z \sim 0.5$ (typically $M_B^* + 2$) and even less with those at $z \lesssim 0.2$ ($M_B^* + 5$), but this will be shown to be only partially true. The early-type galaxies tend to lie in the upper ranges of luminosity at a given redshift, but this is certainly (at least in part) attributable to a selection bias—absorption features are more difficult to identify in less luminous galaxies, particularly at higher redshifts where the strongest features (Ca II H + K, G band, etc.) can coincide with intense night-sky emission lines.

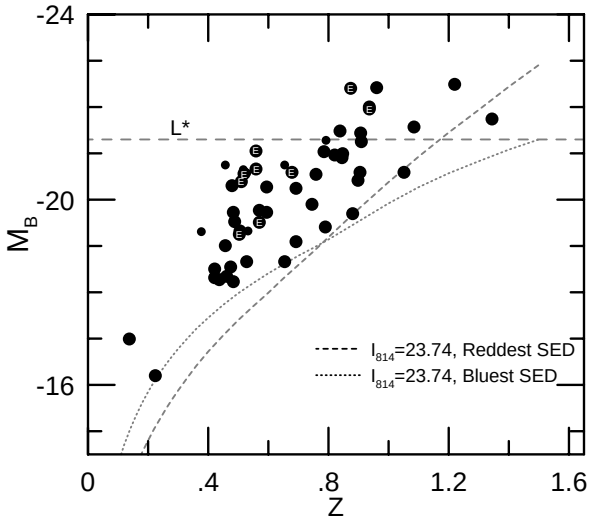

FIG. 6.—Derived B luminosities as a function of redshift. Our effective limit of $I_{814} \lesssim 23.74$ is indicated for two extreme model SEDs. Our sample of compact galaxies spans a wide range in luminosity, indicating that we are probably not dealing with a homogeneous group of galaxies.

3.4. *Size versus Luminosity*

Physical properties of galaxies (size, mass, luminosity) tend to follow certain scaling relationships, and we can use these to probe the nature of the compact galaxies. In Figure 7, we plot B luminosity against the half-light radius in kiloparsecs. These physical radii are based on the major-axis angular radii, $a_{1/2}$, corrected for PSF effects as discussed in § 2.4 above. Also plotted are representative values for local galaxies: luminous ellipticals and S0s (Bender, Burstein, & Faber 1992), spirals and Magellanic irregulars from the RC3 (de Vaucouleurs et al. 1991), spheroidals (Bender et al. 1992; Vader & Chaboyer 1994) and local H II galaxies (Telles 1995).

We see immediately that the compact galaxies generally fall in the same region of this diagram as the local H II galaxies. For a given luminosity, they are much smaller than Magellanic irregulars. Of course, this is largely a selection effect; the sharp lower bound of the compact galaxies results mainly from the cutoff in surface brightness. Given a reasonable redshift distribution, our selection criteria guarantee that the compact galaxies fall where they do in this diagram.

Also plotted in Figure 7 are the "compact narrow emission-line galaxies" (CNELGs) of Koo et al. (1995) and Guzmán et al. (1996). These are small but luminous H II galaxies, which lie at redshifts $0.1 \lesssim z \lesssim 0.7$. A handful of our galaxies reach the extreme small sizes of the CNELGs for a given luminosity, but most are somewhat larger (i.e., less compact).

Except for the early-type systems, the compact galaxies generally lie well off the sequence defined by the luminous spirals and ellipticals. It is reassuring that the early-type systems fall in the expected region. The largest galaxies in

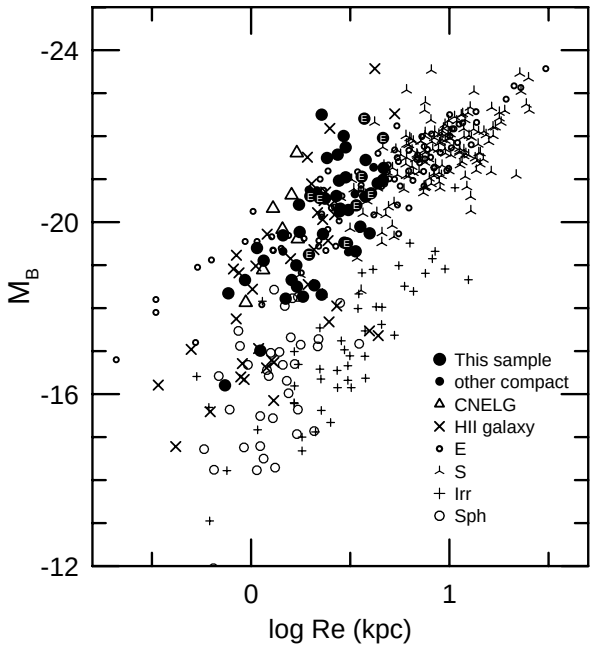

FIG. 7.—Rest frame half-light radii and blue luminosities of our compact galaxies and representative samples of local galaxies of different morphological types. In general, our compact emission line galaxies fall in the same region as local H II galaxies; a few have the extreme compactness of so-called compact narrow emission line galaxies (CNELGs). Some of the larger compact galaxies, including all of the early-type systems, fall near the sequence defined by luminous ellipticals and spirals.

our sample are not necessarily the most luminous, but rather fall in the same region as the early-type systems, consistent with being normal galaxies (disks and bulges) of higher than average surface brightness.

The similarity among the compact galaxies, local H II galaxies, and CNELGs is shown even more clearly in Figure 8, where luminosity is plotted against rest frame average surface brightness. In this figure, the H II galaxies form a broad band offset toward higher surface brightness from the spirals and Magellanic irregulars, with the CNELGs defining the extreme high surface brightness edge. Again, the compacts fall in the H II galaxy regime, spanning the range from the CNELGs to the spirals with the highest highest surface brightness. Note that the upper envelope of the compacts is set primarily by the upper size cutoff, $a_{1/2} \leq 0\farcs5$, and so again results from our selection criteria.

3.5. *Emission-Line Widths*

Widths of emission lines can provide valuable information about the internal kinematics of galaxies. Our spectra allow us to measure line widths as small as ~ 1 Å, corresponding to ~ 40 km s^{-1} at $\lambda_{obs} \sim 7000$ Å (e.g., [O II] λ3727 at $z \sim 0.9$ or [O III] λ5007 at $z \sim 0.4$).

Measuring emission-line widths for these galaxies is complicated, however, by many factors such as seeing, slit width, and small galaxy size, all of which have similar scales for distant galaxies. These problems are discussed in some detail in Rix et al. (1997) and Vogt et al. (1996). The technique we used to measure line widths, described briefly here and in greater detail in Paper II, is very similar to that detailed in Rix et al. For single lines in our spectra (Hβ or [O III] λ5007, for example), we fit the line by a simple Gaussian profile, solving for the best fit in wavelength, amplitude, width, and background. In many cases, only the [O II] doublet at λ5007 was available, and these lines were fitted by a pair of Gaussian profiles whose spacing was fixed at $(1 + z) \times 2.75$ Å.

Finally, we needed to determine an instrumental profile for the LRIS spectra. This is a complicated task, since the slit is resolved, the seeing disk is typically smaller than or comparable to the slit width, and LRIS is slightly undersampled. As an empirical test of the instrumental resolution, we measured narrow absorption features in the spectra of bright stars, which indicated a value of 3.1 Å FWHM. Also, we compared model slit profiles to observed night-sky line profiles, finding that the instrumental FWHM of the LRIS camera (including the anamorphic factor) must be ~ 1.7 pixels. We used this to model an emission line for a galaxy with $r_{1/2} = 0\farcs3$ and zero internal velocity, following the procedure in Vogt et al. (1996, 1997). This model indicated an effective resolution of 3.4 Å, in good agreement with that measured empirically. We have adopted the empirically determined value of 3.1 Å. Note that a larger value for the instrumental resolution would have the effect of making line widths, and thus velocities and masses, smaller. All measured line widths were adjusted by subtracting the instrumental resolution in quadrature and then converted to velocities. Where more than one emission line was available, we calculated a weighted average based on the quality of the individual measurements (see Paper II).

The results are shown in Figure 9, plotted against the physical half-light radius of each galaxy. Since these are all emission-line galaxies, we have split our sample into lower ($z < 0.7$) and higher redshift groups to look for any systematic trend. Again, we show the representative sample of local galaxies and CNELGs for comparison.

In Figure 9, the underlying tracks for galaxy masses (in units of $M_\odot$) assume the virial mass estimation used by Guzmán et al. (1996). This estimate is $M \simeq 3c_2/G\sigma^2 R_e$, where c_2 is a geometry-dependent factor (Bender et al. 1992)

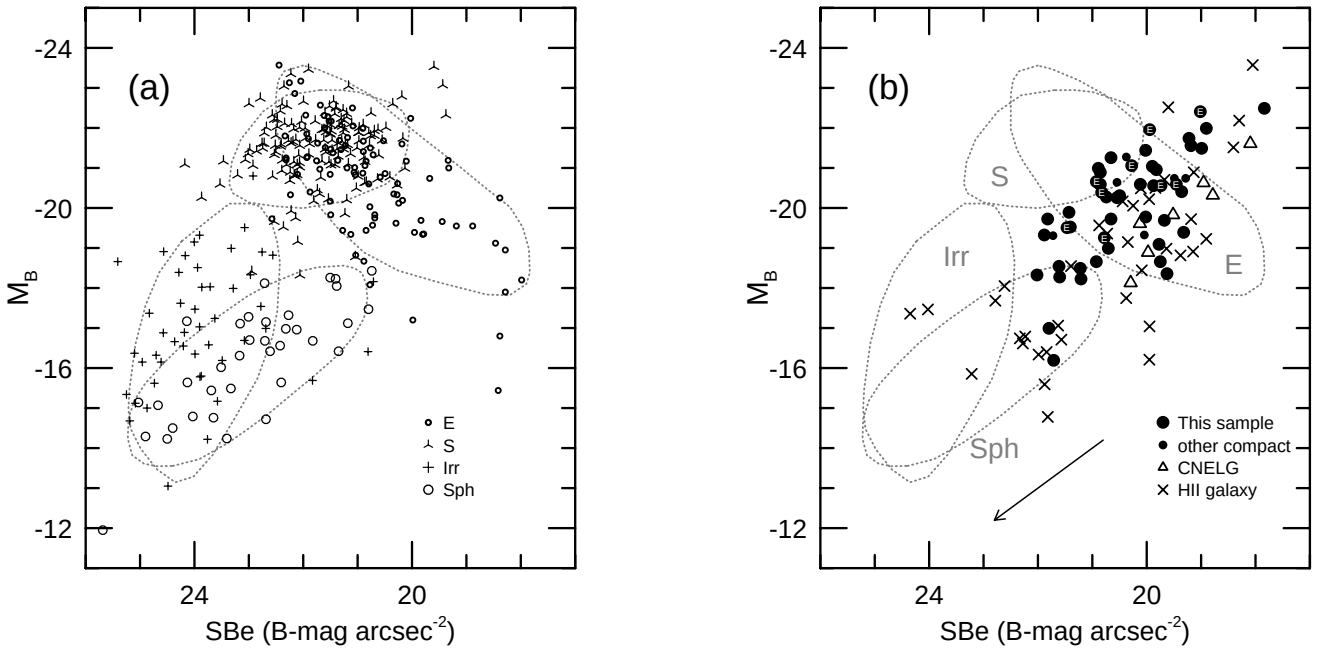

FIG. 8.—Rest frame surface brightness and blue luminosities. The surface brightness is averaged within the half-light radius. For clarity, we have plotted separately (*a*) a local comparison sample (see text) and (*b*) the compact galaxies of the present sample, distant compact narrow emission line galaxies (CNELGs), and local H II galaxies. Dotted lines indicate the general regions occupied by different classes of local galaxies; the arrow in (*b*) represents the direction of simple fading. The compact galaxies form a sequence that crosses the locus of elliptical galaxies and parallels the CNELGs (see text). The galaxies match the locus of local H II galaxies reasonably well.

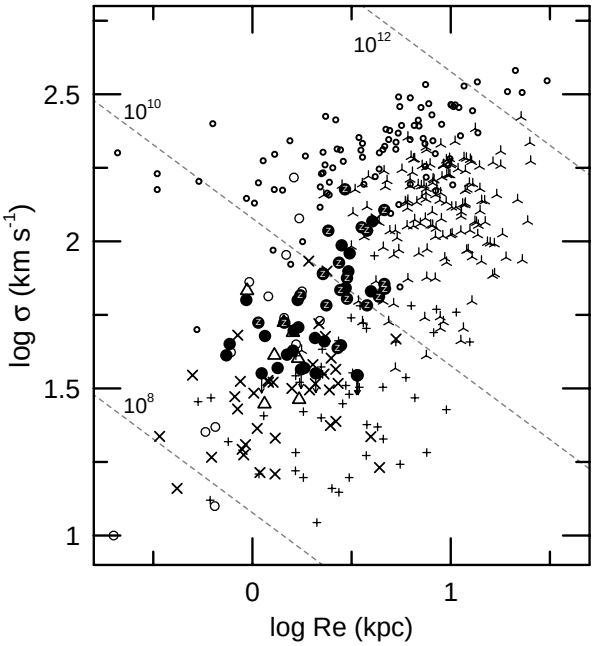

FIG. 9.—Rest frame half-light radii and velocity widths, for those galaxies with measurable emission line widths (45 in total). The line widths have been corrected for instrumental broadening as described in the text. Dashed lines indicate galaxy masses in solar units. Symbols are as in Figs. 7 and 8, with compact objects at $z > 0.7$ marked with Z. The bulk of the compact galaxies at $z < 0.7$ fall in the same region as the CNELGs (*triangles*) and local H II galaxies (*crosses*). Those at higher redshift tend to be more massive on the average, but only a few approach the region of normal spirals.

and R_e is the half-mass radius, which we equate with the half-light radius. Exponential profiles of dwarf systems can be reasonably fitted by a King model with a ratio of tidal to core radii of $\log(r_t/r_c) = 1.2$ (Binggeli & Cameron 1991). For this ratio, the King models of Bender et al. (1992) give $c_2 \simeq 1.6$. Following a similar argument, $r^{1/4}$-law profiles have a value $c_2 \simeq 1.0$. We adopted the exponential case, $c_2 = 1.6$, for our mass estimates.

Observations by Rix et al. (1997) have very similar instrumental parameters and provide a valuable check on these mass estimates. In particular, Rix et al. use Fabry-Perot Hα observations of three local, late-type galaxies, degraded to model their distant galaxy observations, to provide a semiempirical calibration between their line widths and rotational velocities. They derive a mean $\sigma_v/v_{\rm circ} \sim 0.6$. Converting their circular velocity to a disk mass estimate using

$$M \simeq \frac{2}{\pi G} v_{\rm circ}^2 R_{25}$$

(Rubin et al. 1985) and approximating $R_{25} \sim 2R_e$, we find that our adopted value of $c_2 = 1.6$ corresponds to $\sigma_v/v_{\rm circ} \simeq 0.52$. This is reasonably close to the semiempirical value of Rix et al., showing that our mass estimate, although derived for virial mass, is not far from that for rotationally supported disks. Since mass depends on the square of the velocities, our mass calculations may be too high by a factor of ~ 1.4 compared to those using the Rix et al. calibration—that is, adopting the Rix et al. calibration would reduce our derived masses.

Figure 9 shows that the compact emission-line galaxies in our sample span an apparent mass range from about $M \sim 3 \times 10^9$ to $2 \times 10^{10}\ M_\odot$, extending from the region occupied by low-mass H II galaxies and irregulars to that of low-mass spirals. Again, many compact galaxies overlap the locus of the CNELGs. Compact galaxies at $z \gtrsim 0.7$ tend to be more massive on the whole, but there is considerable overlap between higher and lower redshift objects. Figure 9 supports the conclusion that the majority (two-thirds) of the emission-line galaxies in our sample are similar to local H II galaxies, with the others likely to be small disk systems.

Note that the position of a point in this diagram is independent of the mass-to-light ratio of the stellar population, provided the star formation has a distribution similar to any underlying population; only evolution in size and/or mass would affect the location of a galaxy in this figure. However, underlying populations are usually larger than regions of intense star formation in starburst and H II galaxies, so fading may produce an increase in R_e (see Lehnert & Heckman 1996) if the currently observed starburst is centrally concentrated.

Finally, we present a mass-to-light diagram for the emission-line galaxies in Figure 10. Masses have been estimated as discussed above, assuming that velocity widths are indicative of the galaxy mass (see Guzmán et al. 1996; Rix et al. 1997; Paper II). However, the validity of this assumption does not affect comparisons between different classes of galaxies, since all have been treated with the same mass estimation methods. Figure 10 confirms what we would expect from Figures 7 and 9, viz., that the mass to light ratios of our galaxies are generally similar to those of local H II galaxies, with a few in the extreme range populated by CNELGs. If we interpret this latter group ($M/L \simeq 0.1$) as CNELGs, we see that our sample extends the population of CNELGs to masses of $10^{10}\ M_\odot$. Once again, about one-third of our galaxies appear to be less extreme than the local

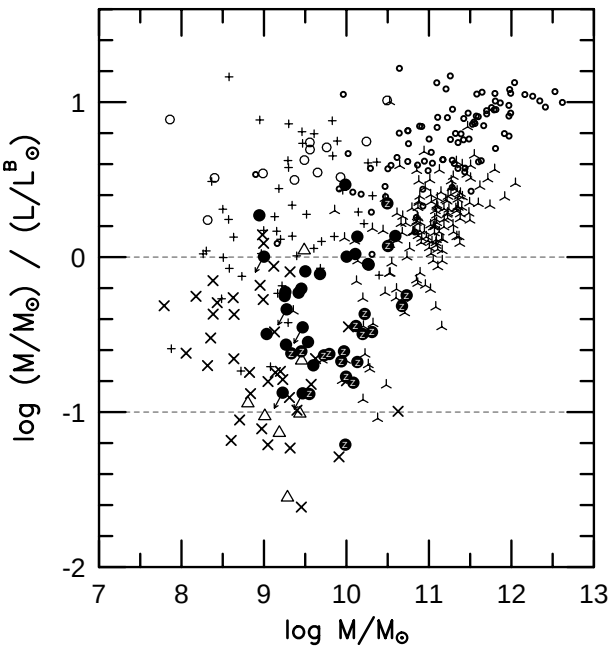

FIG. 10.—Derived masses and mass to luminosity ratios for the same sample galaxies as in Fig. 9. Our galaxies span the range $0.1 \lesssim M/L \lesssim 1$, in solar units (*dashed lines*). Symbols are as in Fig. 9, including H II galaxies (*crosses*), CNELGs (*triangles*), HDF compact galaxy (*filled circles*; those at $z > 0.7$ also marked with Z). The compact galaxies with M/L comparable to the CNELGs reach masses and luminosities about 3 times higher than previously observed in the CNELGs.

H II galaxies, approaching the mass-to-light values of normal disk galaxies, ~1–3 (Faber & Gallagher 1979). Both Figures 9 and 10 show all of our galaxies with measurable emission lines, including four weak-lined galaxies classed above as early-type. Three of these four fall in the more massive, $M/L \sim 1$ region, and the other lies quite near the $M/L \sim 0.1$ line. This latter case (sw3_1378_0453) shows a reasonably high ellipticity, 0.32, so its small velocity width almost certainly indicates low mass rather than a projection effect. Its major-axis profile is clearly exponential, and its V_{606}–I_{814} color is bluer than that of any of the other early-type galaxies. The relative weakness of the emission lines may be due to a poststarburst nature.

3.6. *Summary of Properties*

The major points from the preceding sections are the following:

1. Approximately 15% of our observed compact galaxies are normal early-type galaxies at $0.4 < z < 0.9$. Correcting for the bias against bright ellipticals in our sample raises the fraction to ~23%. It is likely that the true fraction is somewhat larger, up to ~33%, if we account for the unidentified objects.
2. Approximately 70% are emission-line galaxies. Of these, about two-thirds appear to be relatively low-mass H II galaxies; the others are consistent with being small, high surface brightness disk galaxies. Correcting for the excluded elliptical sample, the fraction is reduced to ~64%.
3. Three objects (~5%) are galaxies at high redshift ($z > 2$) or dominated by an AGN.
4. Only two of our galaxies (~3%) are low-luminosity systems with $M_B \geq M^* + 3$.
5. Only three galaxies (~5%) fall in the range $z \lesssim 0.4$.
6. Galaxies in the range $1.4 \lesssim z \lesssim 2.2$ cannot account for more than ~10% of our observed compact sample.

4. DISCUSSION

4.1. *Fraction of Low-Redshift Compact Galaxies*

The basic properties of the compact galaxies rule out a large fraction of low-luminosity, high–surface brightness galaxies at low redshift. This is not surprising, since our cutoff in angular size corresponds to a very small physical size at low redshift; however, such small, low-z objects would suffer little cosmological dimming and so would be biased toward inclusion in our sample if they existed. Recall that the original observed sample included objects of $r_{1/2} > 0\farcs5$, but only two out of the 11 of these we observed were at low z (0.070 and 0.137). We conclude that if a large population of low-z, low-luminosity galaxies exists at these magnitudes, most of these cannot have high intrinsic surface brightness. This finding is in keeping with most locally dwarf-rich models, which generally argue that low-z dwarfs are missed in surveys because they have low surface brightness and thus faint isophotal magnitudes (see, e.g., Driver et al. 1994; Phillipps & Driver 1995; Ferguson & McGaugh 1995). On the other hand, Im et al. (1995) have suggested that their "small exponential ellipticals" (which they associate in part with the compact galaxies of Griffiths et al. 1994) might be low-luminosity dwarfs with $M_{B_J} > -17$. While the surface brightness of their galaxies, with $I_{785} < 20.5$ and $r_{1/2} < 0\farcs7$, would easily place them within our compact sample, we see few examples in our sample of galaxies of such low intrinsic luminosity.

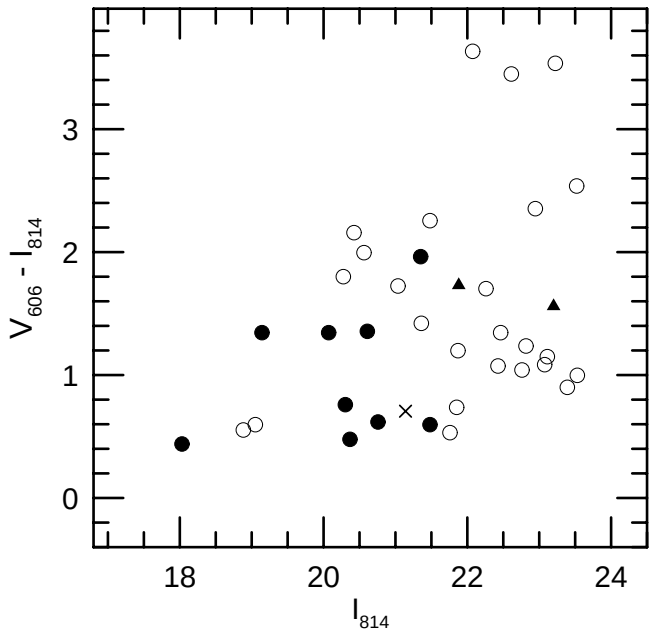

FIG. 11.—$V_{606} - I_{814}$ colors for starlike objects (*open circles*) excluded from our pool of compact objects. The objects with spectroscopic identifications are indicated with filled symbols; all are confirmed to be stars. We also plot the two stars which were found in our compact sample (*filled triangles*) and the location of the one AGN observed in our sample (*cross*). We would expect AGNs to appear among the bluest objects in this plot. It is unlikely that we rejected a large number of AGNs or compact galaxies by excluding starlike objects from our sample.

4.2. *Frequency of AGNs*

Only one galaxy dominated by an AGN was detected in our sample, implying that such galaxies are not common. Our sample could be biased against strong AGNs: if the AGN were several times more luminous than the host galaxy, we might have mistaken it for a star and excluded it during the selection process. Some insight into this comes from the colors of the rejected stellar objects, shown in Figure 11 along with the two confirmed stars and the AGN in our sample. Eleven of these rejected stellar objects were observed by Cohen et al. (1996) and L. L. Cowie (1996, private communication) (nine of which have colors measured by us), and all turned out to be stars. We would expect AGNs to have relatively blue colors (see, e.g., Hall et al. 1996), so it appears likely that only a few of the presumed stars could actually be AGNs[6]. In Figure 11, only four unconfirmed "stars" lie in the blue region where we might expect missed AGNs to be found; this means that, at most, $4 \times (63/245) \simeq 1$ AGN could be missing from our sample.

Using emission-line diagnostics, Tresse et al. (1996) found that at least 8% of galaxies at $z < 0.3$ in the Canada-France Redshift Survey (CFRS) display evidence of "activity," that is, evidence for an ionizing source other than young stars. While analysis of line ratios is deferred to Paper II, the identification of only one AGN (based on broad Mg II

[6] The same question could be asked about extremely compact galaxies being rejected as stars. Some galaxies in our sample have $V_{606} - I_{814}$ colors up to ~2 mag, and some presumed stars have colors this red. However, our angular size cutoff for exclusion of stars must have been fairly conservative, as no galaxies have yet been found among the excluded starlike sample, whereas two field stars were found among our selected galaxy sample.

emission) in our higher redshift sample does not support a rate of $\geq 8\%$, which would mean at least four such objects out of the 52 galaxies at $z < 2$. These numbers are clearly subject to small number fluctuations, however. We also note that two galaxies in our sample show weak, narrow Mg II in emission (see Appendix); this might be indicative of AGN-like activity, although an examination of UV spectra of various galaxy classes (Kinney et al. 1993) fails to yield a consistent picture as to what kind of galaxies display such emission.

4.3. *The "Bursting Dwarf" Hypothesis*

Our sample may provide observational evidence for the model of Babul & Ferguson (1996), who propose a mixture of "normal" galaxies (which passively evolve into the local observed galaxy population) and a population of "bursting dwarfs" as hypothesized by Babul & Rees (1992). The Babul & Rees dwarfs arise in "minihaloes" of mass $\sim 10^9$ $M_\odot$, where gas is gravitationally bound but star formation is delayed until $z \lesssim 1$. When star formation does take place, a single burst (10^7 yr) is followed by the expulsion of the remaining gas by supernovae, and the galaxy fades. These bursting dwarfs may explain the excess of faint blue galaxies (see, e.g., Kron 1980; Tyson 1988). Because these bursting dwarfs are physically small ($R_e \sim 1$ kpc) but luminous, they should be well represented in our sample.

Do we observe such galaxies? Babul & Ferguson (1996) give these plausible characteristics for the bursting dwarfs: masses 0.6–7.5 $\times 10^9$ $M_\odot$; $R_e \sim 0.8$–2.0 kpc (about 30% larger following the expulsion of gas); and peak luminosities -16.5 to -19.3 M_B, or ~ 0.6–8 $\times 10^9$ $L_\odot^B$. These properties are outlined in Figure 12. We see that the smallest quarter of our galaxies fall into this region. (If $q_0 = 0.5$ instead of 0.05, both the radii and luminosities of our compact objects become smaller, by 11% and 0.25 mag at $z = 0.5$, or 20% and 0.47 mag at $z = 1$, placing a few more objects into the specified range.) However, most of our objects—even most of the emission line galaxies—fall outside the bursting-dwarf range, being in general too large and luminous. Figure 6 shows that all the objects at redshifts $z \gtrsim 0.8$ are more luminous than the model dwarfs, and many of those at lower redshifts also exceed the upper luminosity.

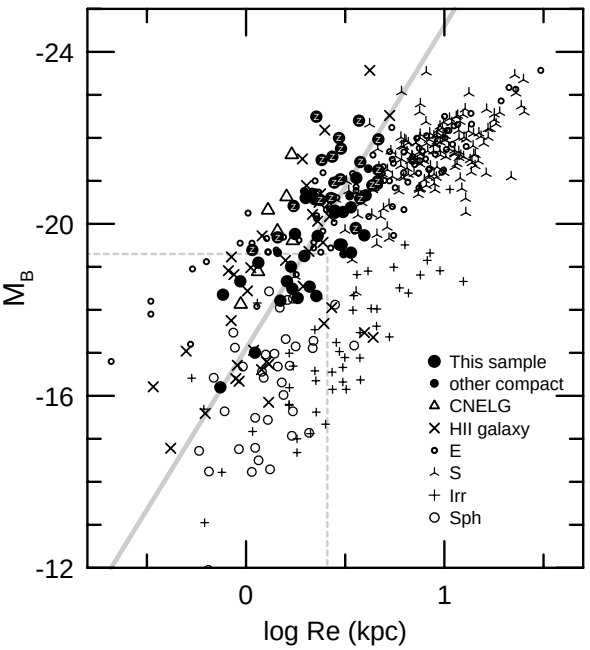

FIG. 12.—Same as Fig. 7, but with the high-redshift ($z > 0.7$) galaxies marked (Z), and overlaying the Babul & Ferguson (1996) size-luminosity relation (*gray line*) and the region of their proposed dwarf galaxy parameters (*dashed lines*).

From Figure 10 of Babul & Ferguson (1996), we may estimate the expected fraction of bursting dwarfs in a representative $I_{814} < 23.74$ sample whose magnitude distribution matched that of our sample. This fraction is found to be $\simeq 15\%$ of all galaxies (irrespective of angular size). Working in 0.5 mag bins, we estimate that, if the bursting dwarfs all belonged to our compact galaxy pool, we should see 32 such dwarfs. (On the other hand, if the surface brightness distribution of the bursting dwarfs were the same as that of our total $I_{814} < 23.74$ catalog, we should see six.) The number of galaxies with the size and luminosity of bursting dwarfs that we actually observe is 11–14, a number too low by a factor of 2–3. This number may be consistent with the Babul & Ferguson (1996) model if the pool of compact galaxies is biased to include a large percentage, but not all, of the bursting dwarfs. On the other hand, it is likely that Babul & Ferguson have somewhat overestimated the number of dwarfs needed by adopting a nonevolving population for the rest of the galaxies, whereas some evolution in that population is both expected from evolution models and observed in late-type galaxies (see, e.g., Driver et al. 1995a, 1995b; Glazebrook et al. 1995; Abraham et al. 1996).

It is interesting to consider those compact galaxies that are too luminous to fit the bursting dwarf model. In Figure 12, we have shown the standard relationship adopted by Babul & Ferguson (1996) for the dwarfs, namely,

$$R_e \propto M^{1/3} \propto L^{1/3} ,$$

and calibrated to their galaxies at peak luminosity. This relationship fits our compact galaxies quite well. The majority of our compact galaxies are therefore consistent with starbursting galaxies, but with masses and luminosities an order of magnitude greater than those allowed by the Babul & Ferguson model. We also note that the CNELGs and many of our galaxies lie above the line, demonstrating that galaxies such as CNELGs have even higher surface brightness (i.e., more intense global starburst) than the proposed bursting dwarfs. The origin of such objects—what triggered the bursts—remains an interesting question.

Babul & Ferguson (1996) list a number of critical tests for their model. The only one we might be able to test is the redshift distribution. The major prediction of the model is a sharp increase in faint blue galaxies at $z \lesssim 1$, where conditions first permit the collapse of gas in the minihalos and bursts can occur. The model also predicts a peak at $z \lesssim 0.1$ that consists of faded dwarfs, but these will all be low–surface brightness objects and thus missing from our sample. At first glance, the sharp cutoff in redshift at $z \simeq 0.95$ (Fig. 4) might be interpreted as supporting the model. As noted above, Figure 6 shows that we are not sensitive to Babul & Ferguson dwarfs, whose peak luminosities are $M_B \sim -19.3$, beyond $z \sim 0.8$; that is, we are not sampling the relevant redshift range to see the sharp turn-on of bursting dwarfs. Therefore, the redshift distribution of the compact galaxy sample does not test the specific Babul & Ferguson (1996) model. Since the apparent drop in the redshift distribution at $z \gtrsim 0.95$ is seen among all

galaxies, not just the compacts, it is likely caused by selection biases in redshift identification, as discussed in § 3.2.

In summary, we find evidence for a population of bursting dwarfs similar to those discussed by Babul & Ferguson (1996), but we find that the number of them in our sample is too low by a factor of 2–3 to strictly support the Babul & Ferguson model. We are unable to test the redshift distribution of the model with the current sample.

4.4. *Comparison with Other Studies*

There have been several recent studies of kinematics in faint field galaxies, mostly dealing with galaxies that are spatially well resolved, at least on *HST* images. Vogt et al. (1996, 1997) have measured velocity curves for a total of 17 disk-dominated galaxies at redshifts $0.3 < z < 1$. Forbes et al. (1996) sampled emission-line widths in disk galaxies at similar redshifts. Both of these studies found evidence for only modest increases in luminosity for given rotation velocities compared to local galaxies. On the other hand, Simard & Pritchet (1997) found evidence for luminosity increases of $\sim$1.5–2.0 mag in a strong-[O II]–selected sample for which they could spatially resolve emission lines with the Canada-France-Hawaii Telescope (CFHT). Their galaxies had redshifts of $z \sim 0.35$ and had velocities comparable to those of local sub-L^* galaxies. However, none of these studies included compact galaxies as we have defined them. Three of the Simard & Pritchet galaxies might have been included in our sample if they had been at $z = 0.7$; two of these show significantly high luminosities for their velocities compared to local galaxies, and the other shows significantly low luminosity. The remaining galaxies actually show a somewhat higher offset to greater luminosities than the potential compact galaxies.

The most relevant kinematical study is that of Rix et al. (1997), who measured [O II] line widths in a sample of blue sub-L^* galaxies at $z \sim 0.25$. They concluded that the galaxies in their sample exhibit a $\sim$1.5 mag increase in blue luminosity relative to comparable local galaxies. It is interesting that our sample galaxies have surface brightnesses roughly 1.7 ± 0.9 mag brighter than spirals and Magellanic irregulars of comparable luminosity (Fig. 8). Since Rix et al. selected their sample on photometric criteria only, we might speculate that their sample contained a significant fraction of compact galaxies, which are also predominately blue and have a low M/L ratio. While this remains a possibility, a limited number of *HST* images of a similarly selected sample show mostly well-resolved disk galaxies (P. Guhathakurta 1997, private communication).

Other evidence for brightening of galaxy disks at earlier epochs has been found by Schade et al. (1995, 1996b, 1996c). The half-light radii of the Schade et al. disks are generally, but not exclusively, larger than those of the compact galaxies. Since reliable measurements are difficult to make for compact galaxies from ground-based observations, we limit our detailed comparison to the galaxies observed with *HST* by Schade et al. (1995). Two of the 15 disk-dominated galaxies in that sample fit our selection criteria, assuming the usual ratio of exponential scale length to half-light radius. These two galaxies are the two most deviant points with respect to the local size-luminosity relationship and contribute $\sim$0.3 mag to the increase in surface brightness found by Schade et al. (1995).

Ground-based studies described in Schade et al. (1996a, 1996b) are consistent with this picture—a large number of their galaxies ($\sim$20%–30% of the total Schade et al. 1996c $z > 0.5$ sample) would fall under our compact galaxy classification, and these are the objects showing the greatest deviation from the local relation. If such galaxies are removed from the sample, the amount of brightening is significantly reduced, although not quite enough to be consistent with the modest levels found by Forbes et al. (1996) and Vogt et al. (1996, 1997). Schade et al. (1996c) point out the increase in volume density of luminous small disks at higher redshift, and the data of Schade et al. (1996b, 1996c) suggest that the strongest increase in surface brightness occurs with the smallest disks (also see Simard & Pritchet 1997). We associate these small disks with galaxies in our sample, which we also associate with H II galaxies.

In summary, we have explored a hypothesis that compact galaxies could account for some of the differences found in luminosity evolution in several recent studies. There remains no evidence that kinematical studies (Rix et al. 1997; Simard & Pritchet 1997) have been biased by the inclusion of compact galaxies in the samples, although it remains a possibility. On the other hand, it appears compact galaxies are present and exert a significant influence in the samples of field galaxies studied by Schade et al. (1995, 1996b, 1996c).

4.5. *Evolution of Compact Galaxies*

The compact objects in our sample are not a homogeneous group. In general, the early-type systems will not evolve strongly but instead will fade and redden slightly. On the other hand, about half of our sample are emission-line objects that appear to be similar to local H II galaxies, and we would expect these galaxies to evolve rapidly. Star formation could terminate in these galaxies, with the galaxies then fading and reddening significantly as the stellar population ages. If, instead, vigorous star formation continues instead, older stellar populations would accumulate and become increasingly prominent as the galaxies evolve. In either case, these galaxies will not retain the properties of compact galaxies as we have described them. We will focus on the fate of these galaxies.

Continuing the discussion above, Schade et al. (1996c) find comoving volume densities for the smallest luminous disks at $z_{\rm median} \sim 0.73$ to be the same as those for disks $\sim$1.5 mag fainter at $z_{\rm median} \sim 0.28$. Therefore, one possibility is that star formation rates in compacts decline, and they then fade to become small but "normal" disk galaxies. This hypothesis is not well supported by Figures 7 and 8, however. Fading by somewhat more than 1.5 mag would bring the compacts to the edge of the region of the smallest local Magellanic irregulars, but the correspondence is not striking. It is not possible for most of these galaxies to become normal spirals through passive evolution, as seen most clearly in Figure 9 where the location of objects is insensitive to fading.

If compact galaxies are somewhat less extreme examples of CNELGs, they could be the progenitors of spheroidal[7] galaxies, as argued by Koo et al. (1994) and Guzmán et al. (1996) for the CNELGs. This idea is somewhat supported by Figures 7, 8, and 9, at least for the lower redshift objects, but most of the higher redshift objects appear to be too large to evolve into the spheroidals seen today.

[7] Spheroidal refers to low-density, dwarf ellipsoidal galaxies (Kormendy & Bender 1994) like NGC 205, rather than dwarf spheroidals like Carina.

We can easily derive rough comoving volume densities for the galaxies in our sample, and comparison to local volume densities can shed some light on the nature of these objects. However, we caution that these comparisons are highly uncertain because of the small number of objects involved and sometimes rather questionable assumptions. Furthermore, our selection criteria are difficult to apply to local samples for a proper comparison.

There are ~ 13 lower redshift ($0.4 < z < 0.7$, $M_B < -18$) and ~ 8 higher redshift ($0.7 < z < 1.0$, $M_B < -20$) galaxies which we would associate with H II galaxies. Correcting for the sample incompleteness, these give space densities of 3.2×10^{-3} and 1.2×10^{-3} Mpc^{-3}, respectively. For CNELGs, Koo et al. (1994) find roughly a factor of 3.5 change in number for each magnitude of luminosity, and we can use this to estimate the densities for objects with $M_B < -19$ as 0.9×10^{-3} and 4.0×10^{-3} Mpc^{-3}, respectively. Finally, if we adopt a relatively conservative "lifetime" of $\sim 10^8$ yr, then these numbers should be increased by at least a factor of 20, corresponding to the age width for each redshift interval. This gives a total space density of 1.8×10^{-2} and 8.1×10^{-2} Mpc^{-3} for the descendents of the lower and higher redshift populations, respectively. These densities point to a rapidly evolving population, as the numbers fall a factor of 4 between the two redshift intervals. Note the implicit assumption that the galaxies in each group are the same class of object.

For comparison, the local population of H II galaxies has a volume density of $\sim 1.7 \times 10^{-4}$ Mpc^{-3} for $M_B < -18$ (Salzer 1989). This can be compared directly to the observed low-redshift ($z \sim 0.55$) compact galaxy density, 3.2×10^{-3} Mpc^{-3}, and a density of 1.4×10^{-2} Mpc^{-3} for the high-redshift ($z \sim 0.85$) galaxies extrapolated to the same luminosity. All of these densities have errors $\sim 30\%$ from small number statistics alone, and we are assuming that all of the local H II galaxies would meet our compactness criteria at the appropriate redshift. These cautions aside, and assuming again that we are dealing with a single class of galaxies, there is a sharp decline in the density of H II-like galaxies toward lower redshift.

The density of field spheroidals in the local universe can be crudely estimated as follows: within a ~ 50 Mpc^3 volume in the Virgo cluster, Binggeli, Sandage, & Tammann (1985) find 225 spheroidals brighter than $M_B = -13.7$, roughly the level of fading we would expect for the $M_B \sim -19$ compacts undergoing a single burst of star formation. Assuming that Virgo has an overdensity of ~ 600 with respect to the field (Sandage, Binggeli, & Tammann 1985), and that the ratio of spheroidals to all galaxies is 0.39 in the field and 0.60 in Virgo (Binggeli, Tarenghi, & Sandage 1990), this gives a field density of $\sim 5 \times 10^{-3}$ Mpc^{-3}—about 20 times less than that expected for the descendents of the compacts in our sample. This would appear to rule out the majority of our sample galaxies as progenitors of present-day spheroidals. However, we have already noted that most higher redshift compacts are too large (Fig. 9) to evolve into spheroidals, and yet these higher redshift objects dominate the total space density we have derived. These larger galaxies may have a significantly different evolutionary path than the ones of size and mass similar to the spheroidals. The volume density of the smaller compact galaxies is within a factor of 4 of the estimate for the local field population of spheroidals. Given the large uncertainties in our estimates, we cannot rule out the hypothesis that at least some of the compact galaxies in our sample evolve into spheroidals.

Perhaps the most interesting objects in our sample are the relatively massive ($M \gtrsim 10^{9.7}\ M_\odot$) galaxies that have low $M/L \sim 0.1$ similar to local H II galaxies (Fig. 10). The low M/L values suggest very high star formation rates per unit mass; this is confirmed in Paper II. The evolution of these galaxies is unclear—they are somewhat too large to fade into spheroidals, and apparently neither massive nor large enough to become typical spirals. One possibility is that they are disks forming from the center outward, and so the radius of the luminous material and enclosed mass are small compared to present-day spirals, but this explanation is highly speculative and we have no supporting evidence. This class of compact galaxy remains enigmatic.

5. CONCLUSIONS

The major conclusions concerning the nature of compact galaxies in the HDF are as follows:

1. Approximately 23% are normal early-type galaxies at $0.4 < z < 0.9$. It is likely that the true fraction of early-type systems is somewhat larger, up to $\sim 33\%$, if we account for the unidentified objects.
2. Approximately 64% are emission-line galaxies. Among these, about two-thirds appear to be relatively low-mass H II galaxies; the others are consistent with small, high–surface brightness spirals.
3. Approximately 5% are objects at $z > 2$ (two) or galaxies dominated by AGNs (one). This fraction could be larger if such objects have a stellar-like appearance, but there is no evidence in our data to support a large population of such objects.
4. Galaxies in the range $1.4 \lesssim z \lesssim 2.2$ compose no more than $\sim 10\%$ of our observed sample, based on seven objects without redshift identifications.
5. There is only a very small fraction ($\lesssim 5\%$) of low redshift ($z < 0.4$) compact galaxies.
6. About 25% of the compact galaxies have the physical properties (size and luminosity) of bursting dwarfs as predicted by Babul & Ferguson (1996); this number appears too low to be strictly consistent with their model.
7. About 70% of the compact galaxies appear similar to the bursting dwarfs, but with luminosities an order of magnitude higher.
8. Comoving volume densities of those compact galaxies similar to local H II galaxies are very high compared to local values and indicate a strongly evolving population. Their space densities appear too high for all of them to be the progenitors of present-day spheroidal galaxies, but for the smaller compact galaxies, with masses and sizes similar to the spheroidals, the numbers agree to within a factor of a few. However, uncertainties remain too large to draw firm conclusions about compact–spheroidal connections on the basis of volume densities.
9. Compact galaxies may be responsible for some of the large values of disk luminosity evolution found in recent studies (e.g., Schade et al. 1995, 1996b, 1996c). This may help resolve the large discrepancies between these studies and others (e.g., Vogt et al. 1996, 1997) that examined more massive disks.

We thank Caryl Gronwall for helpful discussions and for providing the model SEDs used for k corrections. We are also grateful to Luc Simard for discussions and to the

referee for several helpful suggestions. We thank Judy Cohen for help coordinating our selection of HDF targets to avoid overlap. We are grateful, as always, to the staff of the W. M. Keck Observatory for making these observations possible. Support for this work was provided by NASA through grants AR-06337.08-94A, AR-06337.21-94A, GO-05994.01-94A, AR-5801.01-94A, and AR-6402.01-95A from the Space Telescope Science Institute, which is operated by AURA, Inc., under NASA contract NAS 5-26555. We also acknowledge support by NSF grants AST 91-20005 and AST 95-29098. J. G. acknowledges the partial financial support from Spanish MEC grants PB89–124 and PB93–456 and a UCM del Amo foundation fellowship. J. D. L. acknowledges support from HF 1048.01-93A.

APPENDIX A

REDSHIFTS OF ADDITIONAL OBJECTS

The 1996 April Keck observing run of the DEEP project had several science objectives in the HDF besides the study of compact objects. These other projects are described elsewhere (Lowenthal et al. 1997; Guzmán et al. 1997b; Vogt et al. 1997). Redshifts were obtained for a total of 112 targets, as well as for eight additional galaxies that serendipitously fell on slitlets. As an aid to other researchers, we compile in Table 2 the redshifts of all of the noncompact objects with redshift $z < 2$. Combined with the redshifts in Table 1 and the $z > 2$ objects presented by Lowenthal et al. (1997), these represent all spectral identifications to date by the DEEP group in the HDF and its flanking fields.

APPENDIX B

NOTES ON UNUSUAL OBJECTS

iw3_0817_0556 ($z = 0.960$).—This object is identified as an AGN on the basis of broad (FWHM $\sim$1800 km s^{-1}) Mg II emission. The spectrum also shows narrow [O II] λ5007, [Ne V] λ5007, [Ne III] λ5007, Hδ, and Hγ; presumably there is also a broad component to the Balmer lines, but these fall in the region of intense night-sky lines and the continuum becomes hard to define. There is also a pronounced narrow absorption system at $z = 0.846$, showing the Mg II doublet and Fe II at 2344, 2374, 2383, 2587, and 2600 Å. This redshift matches that of the disk galaxy iw3_0832_0544, whose center is 1.″8 (18 kpc) from the line of sight.

iw2_0547_0293 ($z = 2.990$).—The Lyα line appears asymmetric in emission, with $W_\lambda \sim -4$ Å (rest frame) and a strong Lyα absorption trough to the blue. There is also a good match to absorption lines at 1260, 1303, 1335, 1394, 1403, 1527, and 1549–51 Å. The redshift is derived from a cross correlation with the spectrum of a local starburst galaxy, NGC 1741 (see Lowenthal et al. 1997).

ie2_0623_0190 ($z = 2.269$).—Lyα does not fall in our observed spectral range, but strong absorption lines at 1527, 1549–51, and 1671 Å make this identification secure. There are also good matches with lines at 1260, 1303, 1335, and 1394 Å. The redshifted Fe II lines at 2344, 2374, and 2383 Å fall in the night sky forest and are plausible but not convincing. As above, the redshift is from a cross correlation with NGC 1741.

se2_0021_0728 ($z = 0.845$ and $z = 0.912$).—This object has two distinct sets of spectral lines. The principle identification comes from the semiresolved [O II] emission lines in both cases. The lower redshift system also shows a 4000 Å break and probable weak, narrow absorption of Mg II and Fe II in the (rest frame) UV. There is no evidence for a spatial offset in the [O II] emission. This object is almost certainly a chance superposition of two galaxies widely separated in space but lying along the same line of sight.

oe4_1223_1134 ($z = 0.821$) *and iw4_1212_1333* ($z = 0.880$).—These two galaxies are unusual because they show narrow Mg II $\lambda\lambda$2796, 2804 emission. The first object has clear P Cygni profiles to the lines; the second may also have P Cygni profiles, but the continuum is weaker and we cannot tell with certainty. Both objects have very strong [O II] lines, and strong [Ne III] λ3869 lines; they also show narrow emission lines of Hγ and Hδ.

hd2_1747_0597 = 12:36:46.26 +62:14:05.7 (J2000) ($z = 0.960$).—This object is not part of our compact sample, but we report it here as it is not discussed in any of our other projects. This very red galaxy, whose image shows a sharp core, displays strong Ca II H + K consistent with a late-type stellar population and an emission system that includes [Ne III] λ3869, [Ne IV] λ2423, [Ne V] λ3426, and (relatively weak) [O II]. The most prominent emission feature is broad, complex Mg II $\lambda\lambda$2796, 2804, whose poorly defined peak corresponds to $z \sim 0.969$. Narrow absorption lines of Mg II appear blueward of the peak, at a redshift of $z = 0.958$. This object is a reported radio source (Fomalont et al. 1997).

TABLE 2

REDSHIFTS OF ADDITIONAL HDF AND FLANKING FIELD OBJECTS

Object (1)	α_{2000} (2)	δ_{2000} (3)	z (4)	References and Published Redshifts (5)
ow4_1077_1033.....	12 36 17.589	62 13 45.29	0.534	
ow2_0626_0318.....	12 36 24.328	62 14 55.13	0.639	
iw2_0224_0735	12 36 30.822	62 14 34.61	0.438	
iw2_0306_0578	12 36 33.350	62 14 33.60	0.748	
iw4_0978_0860	12 36 33.524	62 13 20.89	0.845	C96; $z = 0.843$
sw2_0229_0404	12 36 33.679	62 11 57.45	0.459	C96; $z = 0.458$: MZD; $z = 0.458$
iw2_0328_0562	12 36 33.690	62 14 32.09	0.519	
sw2_0702_0493	12 36 35.232	62 11 10.77	0.410	
iw3_0832_0544	12 36 36.807	62 13 46.89	0.846	
se4_0991_1507.....	12 36 37.875	62 09 23.18	0.514	
hd4_1668_2031	12 36 41.220	62 11 41.90	0.585	
iw3_0807_0181	12 36 41.406	62 14 03.81	0.557	
se4_0906_1177.....	12 36 41.673	62 09 44.15	0.845	
hd4_1851_1509	12 36 44.366	62 11 43.23	1.020	
iw3_1429_0217	12 36 44.508	62 13 05.65	0.485	
nw4_0892_1088.....	12 36 45.920	62 15 28.60	0.851	
hd2_1747_0597	12 36 46.260	62 14 05.66	0.961	C96; $z = 0.960$
hd4_0435_0322	12 36 47.460	62 12 53.70	0.681	
hd2_0346_0312	12 36 47.992	62 13 10.05	0.475	C96; $z = 0.475$; MZD; $z = 0.474$
hd4_1263_0384	12 36 48.966	62 12 22.30	0.953	MZD; $z = 0.953$:
hd4_1322_0320	12 36 49.440	62 12 21.20	0.961	
se2_0304_0307.....	12 36 49.557	62 11 13.98	0.475	
nw2_0358_0561.....	12 36 49.891	62 16 38.09	0.504	
se2_0733_0384.....	12 36 51.004	62 10 31.81	0.410	C96; $z = 0.410$
se3_1081_0497.....	12 36 51.527	62 09 55.54	0.136	
hd2_1111_1361	12 36 51.706	62 13 54.78	0.557	C96; $z = 0.557$
hd2_1918_1912	12 36 52.725	62 14 33.04	0	C96; $z = 0$
nw4_1479_0835.....	12 36 52.748	62 14 45.00	0.321	C96; $z = 0.322$
nw3_1257_0726.....	12 36 52.893	62 15 09.62	0.942	
hd2_0840_1957	12 36 55.440	62 13 54.50	1.146	C96; $z = 1.148$
se3_1468_0345.....	12 36 55.716	62 09 26.44	0.420	
hd3_1722_0963	12 36 57.230	62 13 00.60	0.474	C96; $z = 0.474$
ne4_1269_1248	12 37 00.397	62 14 06.90	0.423	C96; $z = 0.423$
hd3_1994_1763	12 37 00.472	62 12 35.67	0.563	C96; $z = 0.562$
ie4_1172_0992	12 37 01.355	62 11 36.73	0.594	
ie4_1304_1007	12 37 01.924	62 11 24.12	0.136	
ie2_0201_0520	12 37 01.939	62 13 24.17	0.410	C96; $z = 0.408$: MZD; $z = 0.410$
ne4_0935_0944	12 37 02.448	62 14 49.59	0.558	
ne4_1237_1018	12 37 03.206	62 14 19.06	0.512	
ie2_0487_0363	12 37 05.620	62 13 04.48	0.109	
ie3_1131_0636	12 37 05.767	62 11 54.76	0.904	
ie 2_0229_0212	12 37 06.110	62 13 33.92	0.753	C96; $z = 0.753$
oe4_0784_1441	12 37 07.537	62 11 13.31	0.472	
ne3_1126_0608	12 37 07.912	62 14 45.56	0.570	
ie2_0706_0279	12 37 07.980	62 12 47.83	0.654	
ne3_1331_0690	12 37 08.032	62 14 23.64	0.563	
ne3_1364_0595	12 37 09.461	62 14 24.51	0.476	C96; $z = 0.476$
oe4_0981_1325	12 37 10.169	62 11 00.06	0.475	
oe4_0995_1287	12 37 10.730	62 10 59.90	0.747	
ne3_1473_0320	12 37 13.676	62 14 25.58	0.475	
oe2_0639_0458	12 37 19.509	62 12 06.06	0.070	
oe2_0659_0273	12 37 22.038	62 12 11.53	0.928	

NOTES.—Col. (1): Object ID: (field, CCD)_(x)_(y), with x and y in pixels. Cols. (2) and (3): J2000.0 coordinates. Units of right ascension are hours, minutes, and seconds; units of declination are degrees, arcseconds, and arcminutes. Col. (4): Redshift. Col. (5): References and published redshifts: C96 = Cohen et al. 1996; MZD = Moustakis, Zepf, & Davis 1996.

REFERENCES

Abraham, R. G., Tanvir, N. R., Santiago, B. X., Ellis, R. S., Glazebrook, K., & van den Bergh, S. 1996, MNRAS, 279, L47
Babul, A., & Ferguson, H. C. 1996, ApJ, 458, 100
Babul, A., & Rees, M. J. 1992, MNRAS, 255, 346
Bender, R., Burstein, D., & Faber, S. M. 1992, ApJ, 399, 462
Binggeli, B., & Cameron, L. M. 1991, A&A, 252, 27
Binggeli, B., Sandage, A., & Tammann, G. A. 1985, AJ, 90, 1681
Binggeli, B., Tarenghi, M., & Sandage, A. 1990, A&A, 228, 42
Broadhurst, T. J., Ellis, R. S., & Glazebrook, K. 1992, Nature, 355, 55
Bruzual, A. G., & Charlot, S. 1993, ApJ, 405, 538
Cohen, J. G., Cowie, L. L., Hogg, D. W., Songaila, A., Blandford, R., Hu, E. M., & Shopbell, P. 1996, ApJ, 471, L5
Cole, S., Aragón-Salamanca, A., Frenk, C. S., Navarro, J. F., & Zepf, S. E. 1994, MNRAS, 271, 781
Coleman, G. D., Wu, C.-C., & Weedman, D. W. 1980, ApJS, 43, 393
Cowie, L. L., Songaila, A., & Hu, E. M. 1991, Nature, 354, 460

de Vaucouleurs, G., de Vaucouleurs, A., Corwin, H. G., Buta, R. J., Paturel, G., & Fouqué, P. 1991, Third Reference Catalogue of Bright Galaxies (New York: Springer)
Driver, S. P., Phillipps, S., Davies, J. I., Morgan, I., & Disney, M. J. 1994, MNRAS, 266, 155
Driver, S. P., Windhorst, R. A., & Griffiths, R. E. 1995a, ApJ, 453, 48
Driver, S. P., Windhorst, R. A., Ostrander, E. J., Keel, W. C., Griffiths, R. E., & Ratnatunga, K. U. 1995b, ApJ, 449, L23
Faber, S. M., & Gallagher, J. S. 1979, AR&A, 17, 135
Ferguson, H. C., & McGaugh, S. S. 1995, ApJ, 440, 470
Fomalont, E. B., Kellerman, K. I., Richards, E. A., Windhorst, R. A., & Partridge, B. P. 1997, ApJ, 475, L5
Forbes, D. A., Phillips, A. C., Koo, D. C., & Illingworth, G. D. 1996, ApJ, 462, 89
Glazebrook, K., Ellis, R., Santiago, B., & Griffiths, R. 1995, MNRAS, 275, L19
Griffiths, R. E., et al. 1994, ApJ, 435, L19
Gronwall, C. 1996, Ph.D thesis, Univ. California Santa Cruz
Gronwall, C., & Koo, D. C. 1995, ApJ, 440, L1
Guiderdoni, B., & Rocca-Volmerange, B. 1990, A&A, 227, 362
Guzmán, R., Gallego, J., Koo, D. C., Phillips, A. C., Lowenthal, J. D., Vogt, N. P., Faber, S. M., & Illingworth, G. D. 1997a, ApJ, 489, 559 [Paper II]
Guzmán, R., Koo, D. C., Faber, S. M., Illingworth, G. D., Takamiya, M., Kron, R. G., & Bershady, M. 1996, ApJ, 460, L5
Guzmán, R., et al. 1997b, in preparation
Hall, P. B., Osmer, P. S., Green, R. F., Porter, A. C., & Warren, S. J. 1996, ApJ, 462, 614
Im, M., Griffiths, R. E., Ratnatunga, K. U., & Saradejini, V. L. 1996, ApJ, 461, L79
Im, M., Ratnatunga, K. U., Griffiths, R. E., & Casertano, S. 1995, ApJ, 445, L15
Kauffmann, G., White, S. D. M., & Guiderdoni, B. 1993, MNRAS, 264, 201
Kennicutt, R. C. 1992, ApJ, 388, 310
Kent, S. M. 1985, ApJS, 59, 115
Kinney, A. L., Bohlin, R. C., Calzetti, D., Panagia, N., & Wyse, R. F. G. 1993, ApJS, 86, 5
Koo, D. C. 1995, in Wide Field Spectroscopy and the Distant Universe, ed. S. Maddox & A. Aragón-Salamanca (Singapore: World Scientific), 55
Koo, D. C., Bershady, M. A., Wirth, G. D., Stanford, S. A., & Majewski, S. R. 1994, ApJ, 427, L9
Koo, D. C., Guzmán, R., Faber, S. M., Illingworth, G. D., Bershady, M., Kron, R. G., & Takamiya, M. 1995, ApJ, 440, L49
Kormendy, J. 1985, ApJ, 295, 733
Kormendy, J., & Bender, R. 1994, in Proc. ESO/OHP Workshop on Dwarf Galaxies, ed. G. Meylan & P. Prugniel (Garching: ESO), 161
Krist, J. 1993, in ASP Conf. Proc. 52, Astronomical Data Analysis Software and Systems II, ed. R. J. Hanisch, R. J. V. Brissenden, & J. Barnes (San Francisco: ASP), 536
Kron, R. G. 1980, ApJS, 43, 305
Lehnert, M. D., & Heckman, T. M. 1996, ApJ, 472, 546
Lowenthal, J. D., et al. 1997, ApJ, 481, 673
Moustakas, L. A., Zepf, S. E., & Davis, M. 1997, ApJ, 474, L1
Oke, J. B., et al. 1995, PASP, 107, 375
Phillipps, S., & Driver, S. P. 1995, MNRAS, 274, 832
Rix, H.-W., Guhathakurta, P., Colless, M., & Ing, K. 1997, MNRAS, 285, 779
Rubin, V. C., Burstein, D., Ford, W. K., & Thonnard, N. 1985, ApJ, 289, 81
Salzer, J. J. 1989, ApJ, 347, 152
Sandage, A., Binggeli, B., & Tammann, G. A. 1985, AJ, 90, 1759
Schade, D., Carlberg, R. G., Yee, H. K. C., López-Cruz, O., & Ellingson, E. 1996a, ApJ, 464, L63
———. 1996b, ApJ, 465, L103
Schade. D., Lilly, S. J., Crampton, D., Hammer, F., Le Fèvre, O., & Tresse, L. 1995, ApJ, 451, L1
Schade, D., Lilly, S. J., Le Fèvre, O., Hammer, F., & Crampton, D. 1996c, ApJ, 464, 79
Simard, L., & Pritchet, C. 1997, in preparation
Steidel, C. C., Giavalisco, M., Dickenson, M., & Adelberger, K. L. 1996, ApJ, 112, 352
Telles, E. 1995, Ph.D. thesis, Univ. Cambridge
Tresse, L., Rola, C., Hammer, F., Stasińska, G., Le Fèvre, O., Lilly, S. J., & Crampton, D. 1996, MNRAS, 281, 847
Tyson, J. A. 1988, AJ, 96, 1
Vader, J. P., & Chaboyer, B. 1994, AJ, 108, 1209
Vogt, N. P., Forbes, D. A., Phillips, A. C., Gronwall, C., Faber, S. M., Illingworth, G. D., & Koo, D. C. 1996, ApJ, 465, L15
Vogt, N. P., et al. 1997, ApJ, 479, L121
Williams, R. E., et al. 1996, AJ, 112, 1335

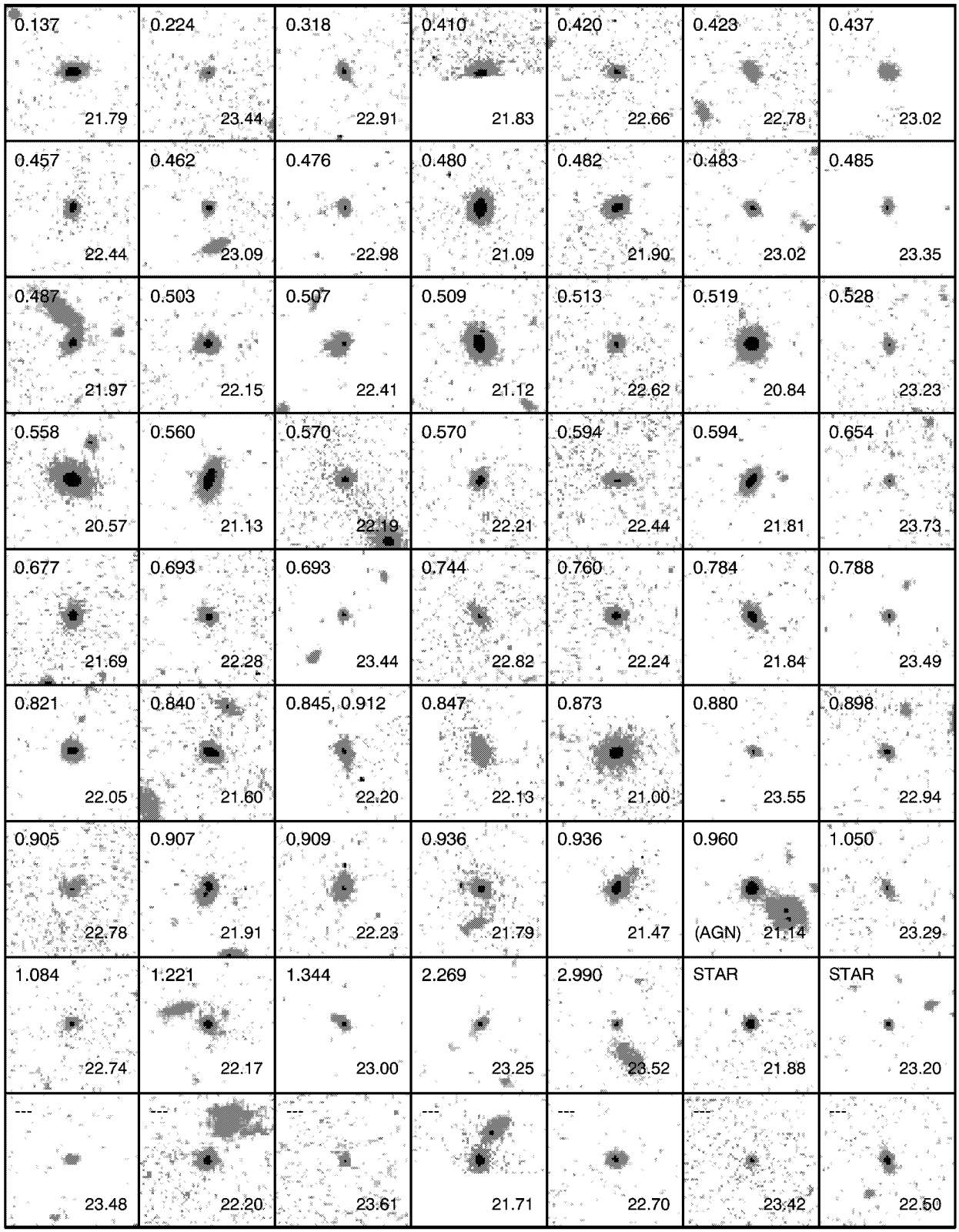

FIG. 3.—*HST* I_{814}-band images of the sample of 63 compact objects. The objects, sorted by redshift, are centered in each box, with the redshift printed in the upper left and total I_{814}-band magnitude in the lower right. Boxes are 6.″0 on a side. The two objects identified as late-type stars are included for comparison with the galaxy images.

PHILLIPS et al. (see 489, 546)